ELSEVIER

Journal of Molecular Structure (Theochem) 620 (2003) 231–255

THEO CHEM

www.elsevier.com/locate/theochem

Conformational dependence of the intrinsic acidity of the aspartic acid residue sidechain in *N*-acetyl-L-aspartic acid-*N*′-methylamide

Joseph C.P. Koo[a,*], Janice S.W. Lam[a], Gregory A. Chass[a,b], Ladislaus L. Torday[c], Andras Varro[c], Julius Gy. Papp[c,d]

[a]*Department of Chemistry, University of Toronto, Toronto, Ont., Canada M5S 3H6*
[b]*Velocet R&D, 210 Dundas St. West, Suite 810, Toronto, Ont., Canada M5G 2E8*
[c]*Department of Pharmacology and Pharmacotherapy, Szeged University, Dóm tér 12, H-6701 Szeged, Hungary*
[d]*Division of Cardiovascular Pharmacology, Hungarian Academy of Sciences and Szeged University, Dóm tér 12, H-6701 Szeged, Hungary*

Received 28 June 2002; accepted 16 August 2002

Abstract

The sidechain conformational potential energy hypersurfaces (PEHS) for the γ_L, β_L, α_L, and α_D backbone conformations of *N*-acetyl-L-aspartate-*N*′-methylamide were generated. Of the 81 possible conformers initially expected for the aspartate residue, only seven were found after geometric optimizations at the B3LYP/6-31G(d) level of theory. No stable conformers could be located in the δ_L, ε_L, γ_D, δ_D, and ε_D backbone conformations. The 'adiabatic' deprotonation energies for the *endo* and *exo* forms of *N*-acetyl-L-aspartic acid-*N*′-methylamide were calculated by comparing their optimized relative energies against those found for the seven stable conformers of *N*-acetyl-L-aspartate-*N*′-methylamide. Sidechain conformational PEHSs were also generated for the estimation of 'vertical' deprotonation energies for both *endo* and *exo* forms of *N*-acetyl-L-aspartic acid-*N*′-methylamide. All backbone–sidechain (N–H$\cdots^{-}$O–C) and backbone–backbone (N–H$\cdots$O=C) hydrogen bond interactions were analyzed. A total of two backbone–backbone and four backbone–sidechain interactions were found for *N*-acetyl-L-aspartate-*N*′-methylamide. The deprotonated sidechain of *N*-acetyl-L-aspartate-*N*′-methylamide may allow the aspartyl residue to form strong hydrogen bond interactions (since it is negatively charged) which may be significant in such processes as protein–ligand recognition and ligand binding. As a primary example, the molecular geometry of the aspartyl residue may be important in peptide folding, such as that in the RGD tripeptide.

Keywords: Aspartate residue; DFT geometric optimization; Deprotonation energy; Hydrogen bond interactions; Sidechain–backbone interactions; Stabilization energy

1. Introduction

1.1. Stereochemical background

N-acetyl-L-aspartate-*N*′-methylamide is the deprotonated form of either the *endo* or the *exo* form

* Corresponding author.
E-mail addresses: joseph.koo@utoronto.ca (J.C.P. Koo), jan.lam@utoronto.ca (J.S.W. Lam), gchass@fixy.org (G.A. Chass), pyro@phcol.szote.u-szeged.hu (L.L. Torday), varro@phcol.szote.u-szeged.hu (A. Varro), papp@phcol.szote.u-szeged.hu (J.G. Papp).

0166-1280/03/$ - see front matter © 2002 Elsevier Science B.V. All rights reserved.
PII: S0166-1280(02)00639-5

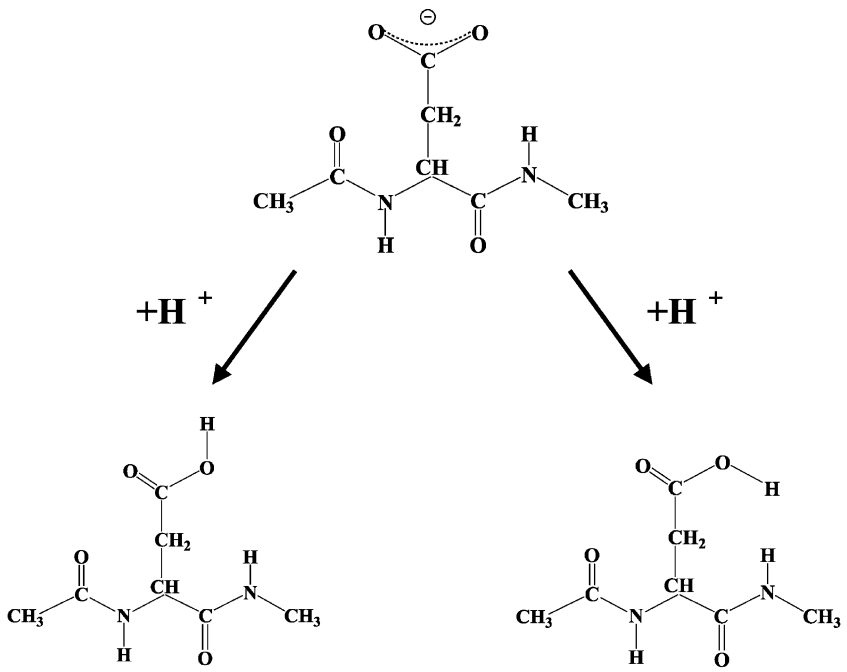

Fig. 1. Protonation of *N*-acetyl-L-aspartate-*N*′-methylamide (top) to the *endo* (bottom left) or the *exo* (bottom right) forms of *N*-acetyl-L-aspartic acid-*N*′-methylamide.

of *N*-acetyl-L-aspartic acid-*N*′-methylamide (Fig. 1). In general, all conformations of an amino acid residue of this complexity may be characterized by at least four torsional angles: ϕ, ψ, χ_1, and χ_2, leading to a potential energy hypersurface (PEHS) consisting of four independent variables (4D) (Eq. (1)):

$$E = E(\phi, \psi, \chi_1, \chi_2). \tag{1}$$

In turn, the 4D PEHS can be separated into two distinctive 2D potential energy surfaces (PESs):

$$E = E(\phi, \psi) \tag{2}$$

$$E = E(\chi_1, \chi_2). \tag{3}$$

Here, Eq. (2) denotes the 2D PES for backbone torsional angles (Ramachandran surface) while Eq. (3) denotes the 2D PES for sidechain dihedral angles. Hence, for *N*-acetyl-L-aspartate-*N*′-methylamide, both backbone and sidechain torsional angles need to be discussed in relation to the overall PEHS so as to describe the molecular geometry of the aspartate residue.

The sidechain of the aspartic acid residue can be modeled by propionic acid (CH_3-CH_2-COOH). When $\chi_3 = 180°$, the aspartic acid residue is capable of sidechain–sidechain (SC/SC) internal hydrogen bonding and it is considered to be in an *endo* orientation (Fig. 2(a)). When $\chi_3 = 0°$, the SC/SC interaction no longer exists and the aspartic acid sidechain is free to participate in external interactions, such as sidechain–backbone (SC/BB) hydrogen bonding. In this case, the aspartic acid residue is considered to be in *exo* orientation (Fig. 2(b)). Unlike aspartic acid, there are no *endo* or *exo* orientations in describing the sidechain characteristic of *N*-acetyl-L-aspartate-*N*′-methylamide. The aspartate anion sidechain can be modeled by propionate ($CH_3-CH_2-COO^-$) where the α-carbon on the aspartate is represented by CH_3.

Here, the carboxylate sidechain of aspartate may exhibit an asymmetric vibrational oscillation about its two C–O bonds, where one bond may be longer, shorter, or of equal length with respect to the other (Fig. 3). In this paper, the longer C–O bond is denoted as r[C–O] and its respective χ_2 torsional angle is denoted normally. On the other hand, the shorter C–O bond is denoted as R[C–O*] and its respective χ_2 torsional angle is denoted as χ_2^*.

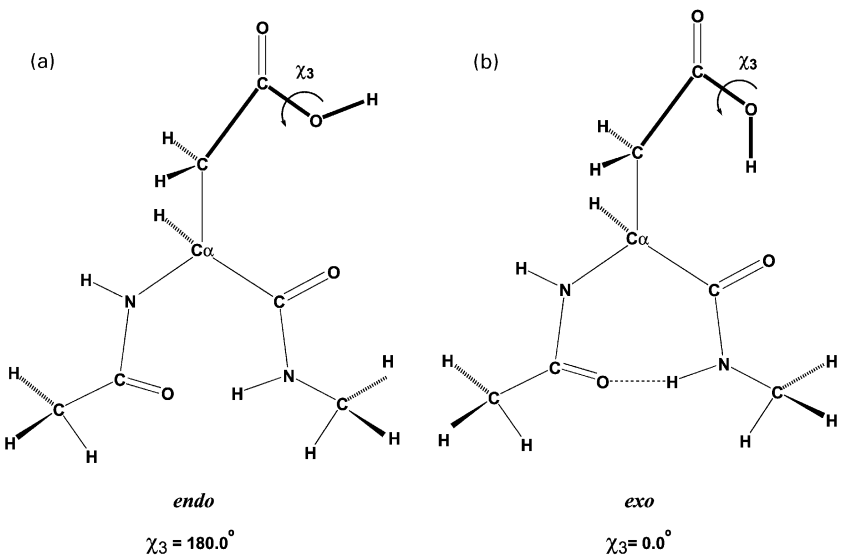

Fig. 2. Definitions of (a) *endo* and (b) *exo* forms of *N*-acetyl-L-aspartic acid-*N*′-methylamide. The sidechain of *N*-acetyl-L-aspartic acid-*N*′-methylamide is modeled by propionic acid.

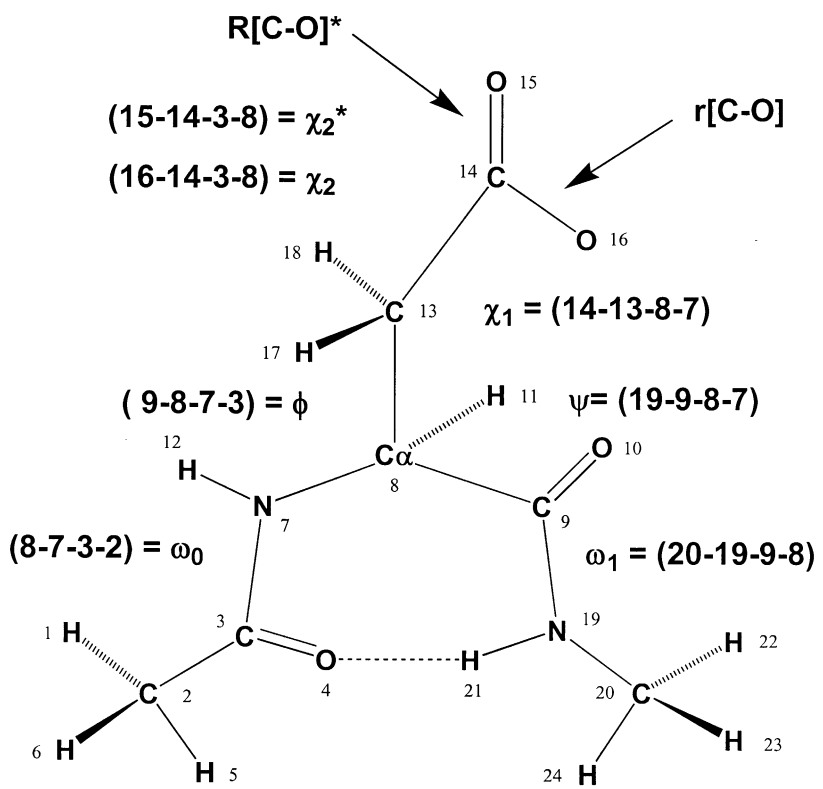

Fig. 3. Definitions of atomic numbering and torsional angles for *N*-acetyl-L-aspartate-*N*′-methylamide.

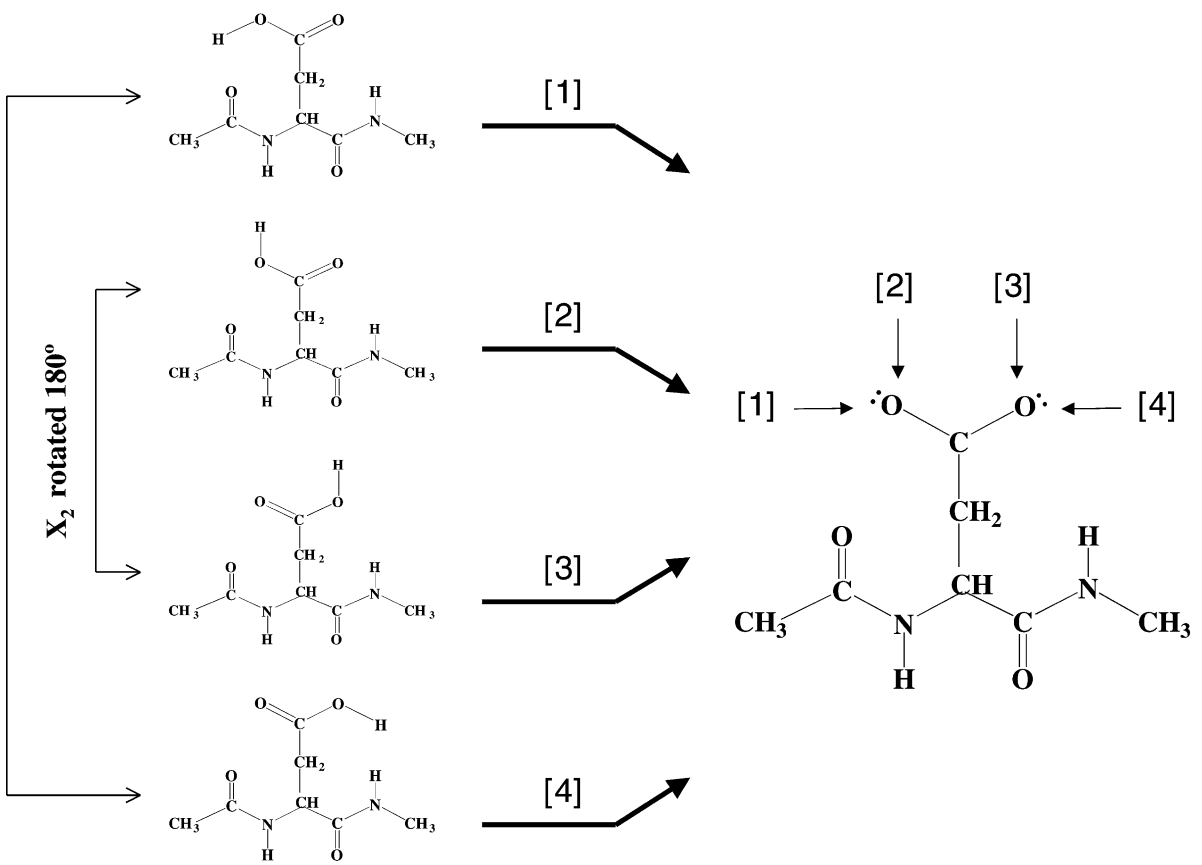

Fig. 4. Protonation choices for *N*-acetyl-L-aspartate-*N*′-methylamide: [1] and [4] depicts the protonated *exo* form while [2] and [3] depicts the protonated *endo* form. The two *exo* forms (and the two *endo* forms) differ from one another by having their χ_2 torsional angles rotated by 180°.

It is interesting to explore the protonation preference for the aspartate anion. Depending on where on the carboxylate sidechain it is protonated, an aspartate anion will transform into the *endo* or *exo* form of its aspartic acid sidechain counterpart. At the end, there could be two *endo* and two *exo* protonation location (Fig. 4). Hence, we propose a protonation model for *N*-acetyl-L-aspartate-*N*′-methylamide where the H atom will protonate each conformer of the aspartate residue at a maximum of four locations. The two possible *endo* protonated forms differs from one another by a χ_2 rotation of 180° (Fig. 4[2] and [3]). Likewise, the two possible *exo* protonated forms differs from one another also by a χ_2 rotation of 180° (Fig. 4[1] and [4]). In this paper, the geometric preference of the aspartate residue will be compared against those of its protonated forms, the *endo* and *exo* conformers of aspartic acid, whose results have been previously published [1,2].

Before, many studies have been performed on single amino acids, including alanine [3–8], asparagine [9], cysteine [10,11], glycine [12,13], phenylalanine [14–16], proline [17], selenocysteine [18], serine [19–21] and valine [22]. Here, the backbone geometry of *N*-acetyl-L-aspartic acid-*N*′-methylamide is similar to that of the alanine residue, where the H atom of the α-methyl group of alanine is replaced by a $-COO^-$ group.

1.2. Biological background

Recently, many mutational studies were performed on receptors and channels in the biological systems. Among these investigations were reports that aspartic

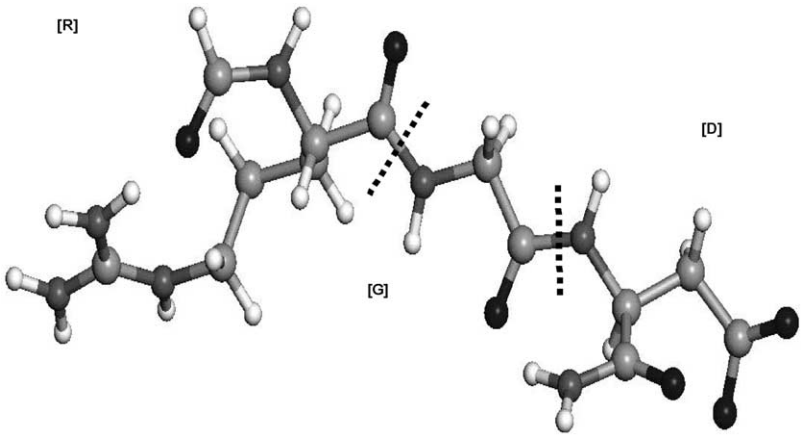

Fig. 5. An example of the arginine (R)–glycine (G)–aspartic acid (D) tripeptide.

acid, or aspartate, is crucial in the selectivity and regulation of ion channel selectivity, ligand binding, as well as functionality of a receptor protein. For instance, it was reported that an aspartic acid site in the inositol 1,4,5-trisphosphate receptor is important in controlling Ca^{2+} selectivity [23]. Also, an aspartate-rich region in the calsequestrin Ca^{2+} binding protein was found to be important in a receptor-mediated Ca^{2+} release process by acting as a direct binding site for Ca^{2+} [24]. In another study, point mutations of the aspartate residue was also found to abolish Ca^{2+} permeation in the epithelial Ca^{2+} channel, causing the channel to be non-functional [25]. Mutations in two aspartate regions of the human immunodeficiency virus-1 (HIV-1) *chemokine coreceptor CXCR4* were even found to be able to reduce HIV-1 entry into host cells [26]. In these cases, the sidechain and backbone geometry of the aspartate residue will result in the formation of various stabilizing forces that may affect the binding affinity or function of proteins and receptors. The aspartate residue is also a key amino acid in many clinical studies involving probing assays [27,28], aging [29,30], cerebral injury [31], and enzyme activities [32] just to name a few. Perhaps one of its most important associations with medicine, however, lies in its connection with the RGD tripeptide (Fig. 5). The arginine (R)–glycine (G)–aspartic acid (D) tripeptide has been intensively studied in molecular biology and medical genetics. It was shown to improve gene delivery efficiency [33,34] and expand the tropism of gene-delivering vectors [35], and increase a drug's oral bioavailability in a body system [36]. By studying the three-dimensional molecular preference for the aspartate residue, insights may be gained in the RGD's binding affinity and geometric characteristics. Since computational molecular modeling of molecules is an area of high interest in recent years in drug designs [37–44], ab initio studies on amino acids such as the aspartate residue may deem beneficial in the pharmaceutical industry; especially when exploring binding affinity or selectivity of a target receptor. In this paper, we wish to report all possible sidechain (SC) and backbone (BB) conformers that may exist for the aspartate residue, using *N*-acetyl-L-aspartic acid-*N*′-methylamide as a peptide model. In addition, the deprotonation and protonation preference for the aspartate residue will be explored. The deprotonation and protonation characteristics of this aspartate will decide the various inter- and intra-residual and intermolecular hydrogen interactions that may result. In turn, these forces may directly govern the binding patterns of ligands to aspartate sites in receptors and proteins.

2. Computational methods

To determine all geometric minima for *N*-acetyl-L-aspartate-*N*′-methylamide on the conformational PEHS, shown in Fig. 6, ab initio optimizations were performed on all possible sidechain conformers in the nine backbone conformation (γ_L, β_L, δ_L, α_L, ε_L, γ_D, δ_D, α_D, ε_D). All calculations were performed using GAUSSIAN 94 [45] and GAUSSIAN 98 [46].

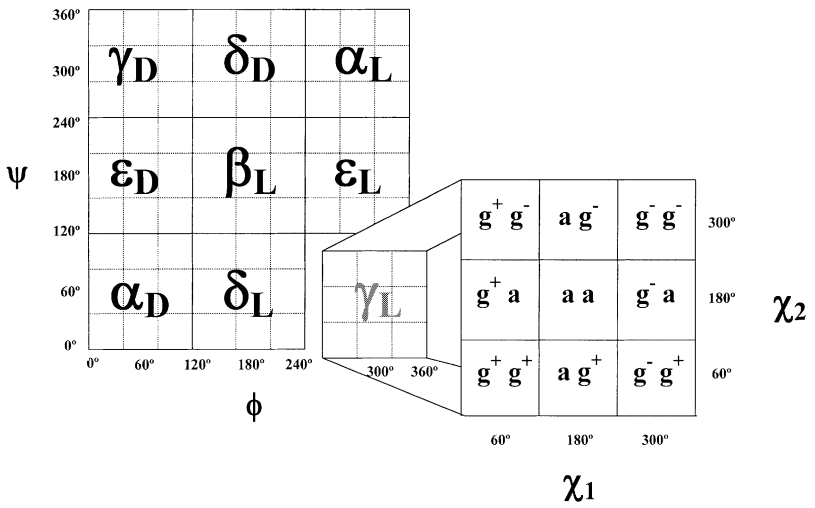

Fig. 6. Schematic representation of the 4D Ramachandran PEHS, $E = E(\phi, \psi, \chi_1, \chi_2)$. Each of the nine backbone conformations (γ_L, β_L, δ_L, α_L, ε_L, γ_D, δ_D, α_D, ε_D) holds nine sidechain conformations as illustrated by the γ_L backbone.

Here, $CH_3-CH_2-COO^-$ was used to mimic the geometric characteristics of the aspartate sidechain. Tight geometry optimizations were performed at RHF/3-21G, RHF/6-31G(d), and B3LYP/6-31G(d) levels of theory using Berny optimization (FOPT = TIGHT, Z-MATRIX). Under these conditions, a gradient of less than 1.5×10^{-5} a.u. was generated at termination for all critical points. Since there could be $3^2 = 9$ structures from backbone conformations (γ_L, β_L, δ_L, α_L, ε_L, γ_D, δ_D, α_D, ε_D) and that there could be $3^2 = 9$ sidechain orientations (χ_1, χ_2), there could exist a maximum of $9 \times 9 = 81$ possible conformers for the aspartate residue at each level of theory. In this paper, only the B3LYP/6-31G(d) results were reported for the optimized geometries.

Partially relaxed PEHS double-scan calculations were performed at the RHF/3-21G level of theory on the backbone conformations in which all stable conformers were found (γ_L, β_L, α_L, α_D) for *N*-acetyl-L-aspartate-*N*′-methylamide. These scan calculations, where $E = E(\chi_1, \chi_2)$, were carried out under normal condition where (FOPT = Z-MATRIX). By setting and specifying the ϕ and ψ torsional angles, the aspartate was fixed to the specified backbone conformations. In addition, the two sidechain variables, χ_1 and χ_2, were rotated with 30.0° increments, resulting in $12 \times 12 = 144$ points. Consequently, all critical points generated in these scan calculations had gradients of less than 4.5×10^{-4} a.u.

The stabilization energy exerted by the sidechain on the backbone was calculated with respect of the γ_L (Eq. (4)) and β_L (Eq. (5)) backbones of *N*-acetyl-glycine-*N*′-methylamide using the following isodesmic reaction quoting only the B3LYP/6-31G(d) energy values:

$$\underset{-456.5375150\ \text{Hartree}}{CH_3-CO-(NH-CH_2-CO)-NHCH_3}{}_{\gamma_L} + \underset{-267.815181\ \text{Hartree}}{CH_3-R} \rightarrow \underset{\text{any conformation}}{CH_3CO-(NH-CHR-CO)-NHCH_3} + \underset{-40.5183829\ \text{Hartree}}{CH_4} + \Delta E^{\text{stabil}}(\gamma_L) \quad (4)$$

$$\underset{-456.5357122\ \text{Hartree}}{CH_3-CO-(NH-CH_2-CO)-NHCH_3}{}_{\beta_L} + \underset{-267.815181\ \text{Hartree}}{CH_3-R} \rightarrow \underset{\text{any conformation}}{CH_3CO-(NH-CHR-CO)-NHCH_3} + \underset{-40.5183829\ \text{Hartree}}{CH_4} + \Delta E^{\text{stabil}}(\beta_L) \quad (5)$$

where CH3–CO–(NH–CH_2–CO)–$NHCH_3$ stands for *N*-acetyl-glycine-*N*′-methylamide in its γ_L or β_L backbone conformation; CH_3-R stands for

$CH_3–CH_2–COO^-$; and $CH_3CO–(NH–CHR–CO)–NHCH_3$ stands for *N*-acetyl-L-aspartic acid-*N*′-methylamide. The two stabilization energy values, calculated with respect to the γ_L or β_L backbone of glycine diamide (from Eqs. (4) and (5)), are shifted with respect to each other by 1.132 kcal/mol (Eq. (6)):

$$\text{B3LYP/6-31G(d)} \quad \Delta E^{\text{stabil}}(\beta_L) - \Delta E^{\text{stabil}}(\gamma_L) = 1.132 \text{ kcal/mol}. \tag{6}$$

Fig. 7 shows how the stabilization energy for a particular conformer is calculated.

Since the global minima for most single amino acid diamides in the gas phase are usually located in the γ_L backbone, $\Delta E^{\text{stabil}}(\gamma_L)$ was favored in stabilization energy calculation in the past. However, it was found that the β_L backbone conformation is highly symmetrical when it is fully extended. As a result, the β_L backbone represents a unique structure on the Ramachandran Map and it is becoming more accepted as a parameter for stabilization energy calculations [47–49].

3. Results and discussions

Shown in Table 1 are all optimized results, which include the dihedral angles, the relative energies as well as the stabilization energies, for all stable conformers found for *N*-acetyl-L-aspartate-*N*′-methylamide. Of the possible 81 initial structures expected to be found for *N*-acetyl-L-aspartate-*N*′-methylamide,

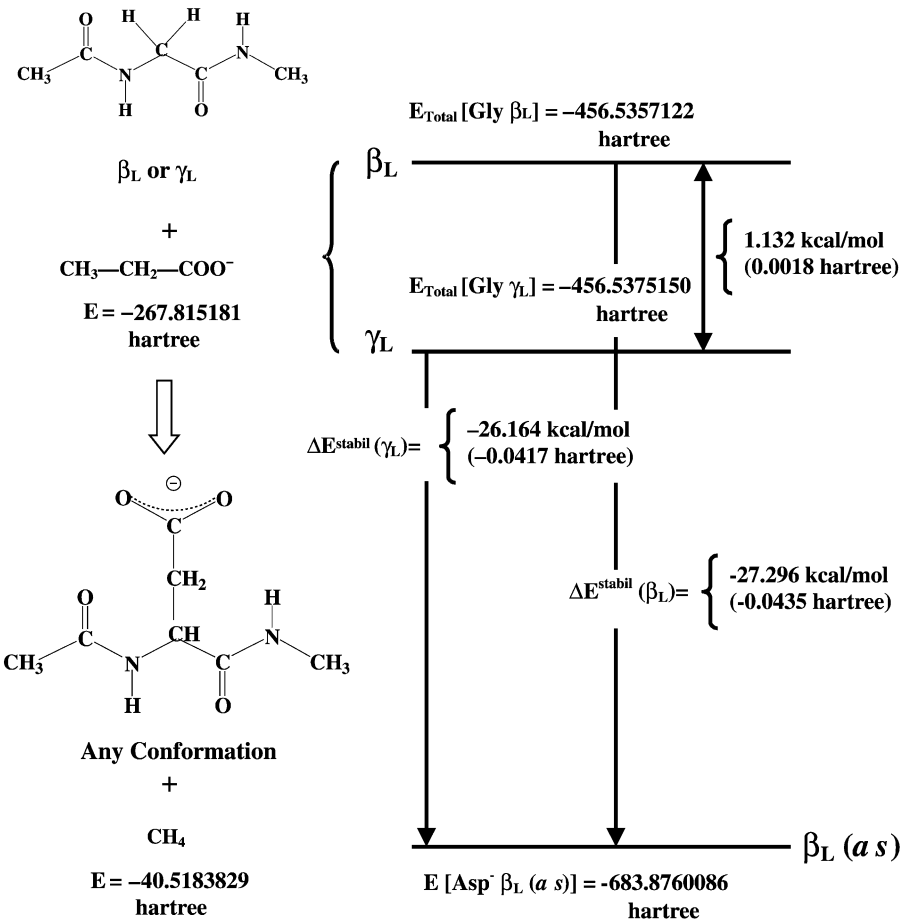

Fig. 7. An example illustrating how the stabilization energy exerted by the sidechain on the backbone was calculated for each conformer of *N*-acetyl-L-aspartate-*N*′-methylamide.

Table 1
Geometric and energetic parameters of optimized conformers of *N*-acetyl-L-aspartate-*N*′-methylamide for all its stable backbone (γ_L, β_L, α_L, and α_D) conformation computed at the B3LYP/6-31G(d) level of theory. Shown here are the optimized torsional angles, computed energy values, relative energies, and stabilization energies

Final conform.	Optimized parameters											
BB [χ_1,χ_2]	ϕ	ψ	ω_0	ω_1	χ_1	χ_2	r[C–O]	χ_2^*	R[C–O*]	E_{min} (Hartree)	ΔE (kcal/mol)	ΔE^{stabil} (kcal) γ_L	ΔE^{stabil} (kcal) β_L
γ_L [g^+s]	−81.09	59.08	−173.78	−177.88	36.39	−24.55	1.281	159.30	1.239	−683.8711687	5.441	−23.127	−24.259
γ_L [g^-g^+]	−80.85	69.00	−165.80	−173.75	−39.99	48.94	1.283	−134.18	1.240	−683.8732396	4.141	−24.427	−25.558
β_L [$a\,s$]	−155.74	174.13	175.95	175.26	−164.36	−12.53	1.279	167.23	1.241	−683.8760086	2.404	−26.164	−27.296
α_L [g^+s^+]	−108.55	−114.69	−172.61	177.10	55.82	105.39	1.262	−71.10	1.261	−683.8755999	2.660	−25.908	−27.039
α_L [g^+s]	−102.59	−53.41	−179.41	−173.68	48.08	−1.22	1.286	179.71	1.238	−683.8798393	0.000	−28.568	−29.699
α_L [g^-g^+]	−70.78	−28.54	−167.10	175.83	−46.91	45.15	1.279	−138.03	1.241	−683.8698728	6.254	−22.314	−23.445
α_D [g^-s]	54.89	41.00	154.07	−167.14	−54.75	21.29	1.281	−159.71	1.242	−683.8613062	11.630	−16.938	−18.070

Note that no stable conformers could be found for the δ_L, ε_L, γ_D, δ_D, and ε_D backbone conformations at this level of theory.

only seven stable conformers were found at the B3LYP/6-31G(d) level. These stable conformers were found in only four of the nine possible backbone conformations: γ_L, β_L, α_L, α_D. The double-scan PEHSs for these backbones reveal numerous minima on the landscape and contour representations, shown in Figs. 8–11. However, only some of these points can be considered as 'true' minima as any minimum found on a particular PES is considered as semi-rigid optimizations. Minima that are not confirmed by subsequent ab initio optimization can only be regarded as 'false' points on the hypersurface and may represent higher order critical points such as those for transition state structures. There are two reasons why false minima occurred on the PEHS for *N*-acetyl-L-aspartate-*N*′-methylamide: (1) both ϕ and ψ torsional angles were frozen during the double-scan calculations; (2) both χ_1 and χ_2 were optimized at fixed 30° increments (from 0 to 360°) while the ϕ and ψ torsional angles were fixed. As mentioned earlier, the backbone geometry of *N*-acetyl-L-aspartate-*N*′-methylamide is expected to be similar to that of the alanyl residue. Since previous ab initio studies on the alanine molecule [3–8] have reported that most stable conformers were found in the γ_L, β_L and γ_D backbone conformations, it is somewhat surprising to learn that no conformers were found in the γ_D backbone of the aspartate residue. Unexpectedly, of the seven stable conformers found for the aspartate residue, three were located in the α_L backbone, a conformation that is not known to harbor stable structures in most amino acids. More surprising, however, is the fact that the global minimum for *N*-acetyl-L-aspartate-*N*′-methylamide occurred in the α_L backbone conformation and not in the γ_L backbone where global minima were usually located. These observations can be linked to the findings by Deane et al. [50], who reported that the α_L region on the Ramachandran plot is readily adopted by the aspartic acid residue in an experiment involving carbonyl–carbonyl interactions.

For this research, it was initially expected that the proton affinity of *N*-acetyl-L-aspartate-*N*′-methylamide could be defined by matching the optimized parameters of stable geometric structures against those optimized in the *endo* and *exo* forms of *N*-acetyl-L-aspartic acid-*N*′-methylamide [1,2]. However, 37 and 27 stable conformers were found, respectively, for the *endo* [2] and *exo* [1] forms of

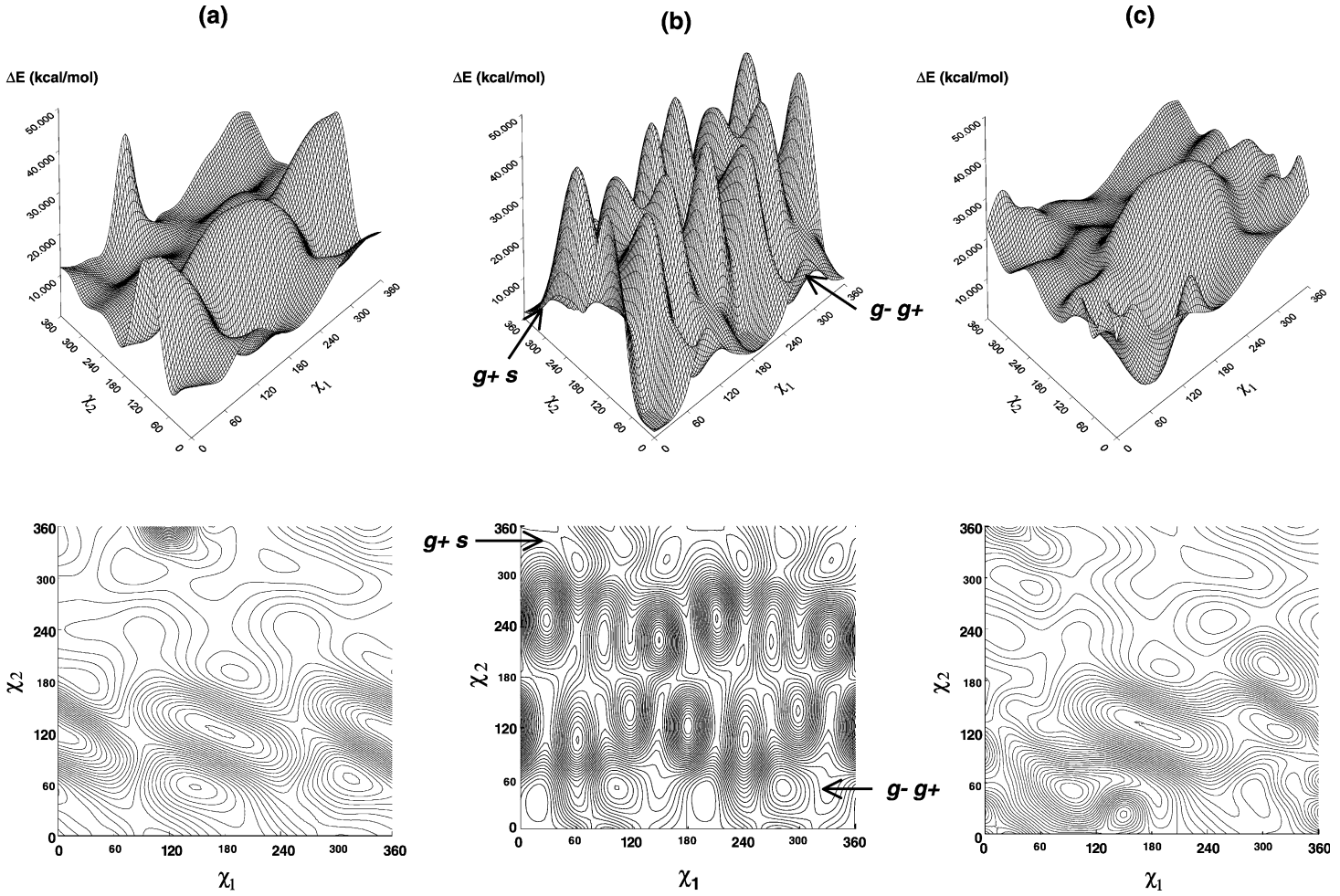

Fig. 8. Double-scan PES, $E = E(\chi_1, \chi_2)$, generated for the γ_L backbone conformation of: (a) the *endo* form of *N*-acetyl-L-aspartic acid-*N*′-methylamide, (b) *N*-acetyl-L-aspartate-*N*′-methylamide, (c) the *exo* form of *N*-acetyl-L-aspartic acid-*N*′-methylamide in both landscape (top) and contour (bottom) representations. Note that the double-scan results for the *endo* and *exo* forms were previously published [1,2]. Torsional angles χ_1 and χ_2 are given in degrees.

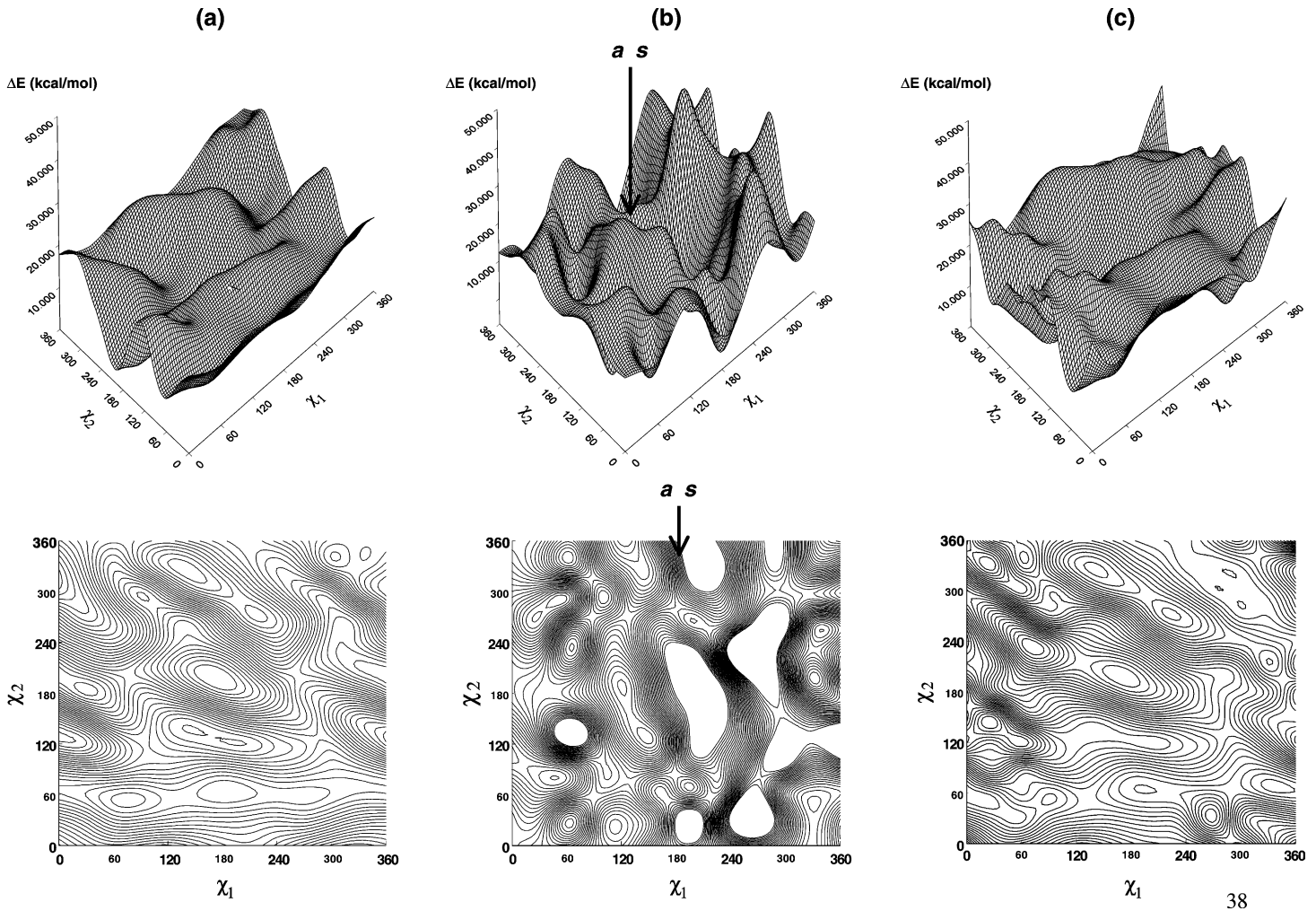

Fig. 9. Double-scan PES, $E = E(\chi_1, \chi_2)$, generated for the β_L backbone conformation of: (a) the *endo* form of *N*-acetyl-L-aspartic acid-*N*′-methylamide, (b) *N*-acetyl-L-aspartate-*N*′-methylamide, (c) the *exo* form of *N*-acetyl-L-aspartic acid-*N*′-methylamide in both landscape (top) and contour (bottom) representations. Note that the double-scan results for the *endo* and *exo* forms were previously published [1,2]. Torsional angles χ_1 and χ_2 are given in degrees.

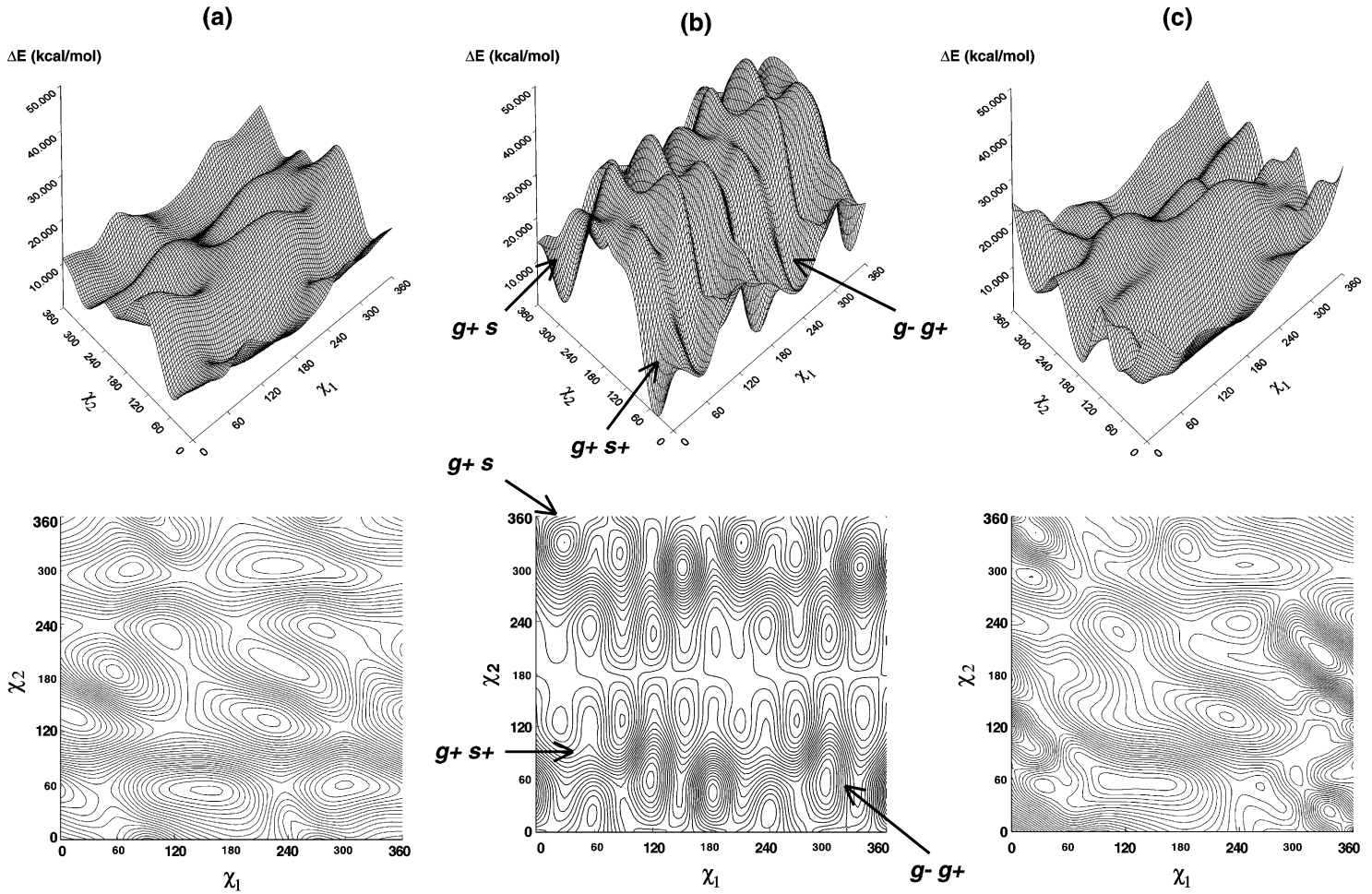

Fig. 10. Double-scan PES, $E = E(\chi_1, \chi_2)$, generated for the α_L backbone conformation of: (a) the *endo* form of *N*-acetyl-L-aspartic acid-*N*′-methylamide, (b) *N*-acetyl-L-aspartate-*N*′-methylamide, (c) the *exo* form of *N*-acetyl-L-aspartic acid-*N*′-methylamide in both landscape (top) and contour (bottom) representations. Note that the double-scan results for the *endo* and *exo* forms were previously published [1–2]. Torsional angles χ_1 and χ_2 are given in degrees.

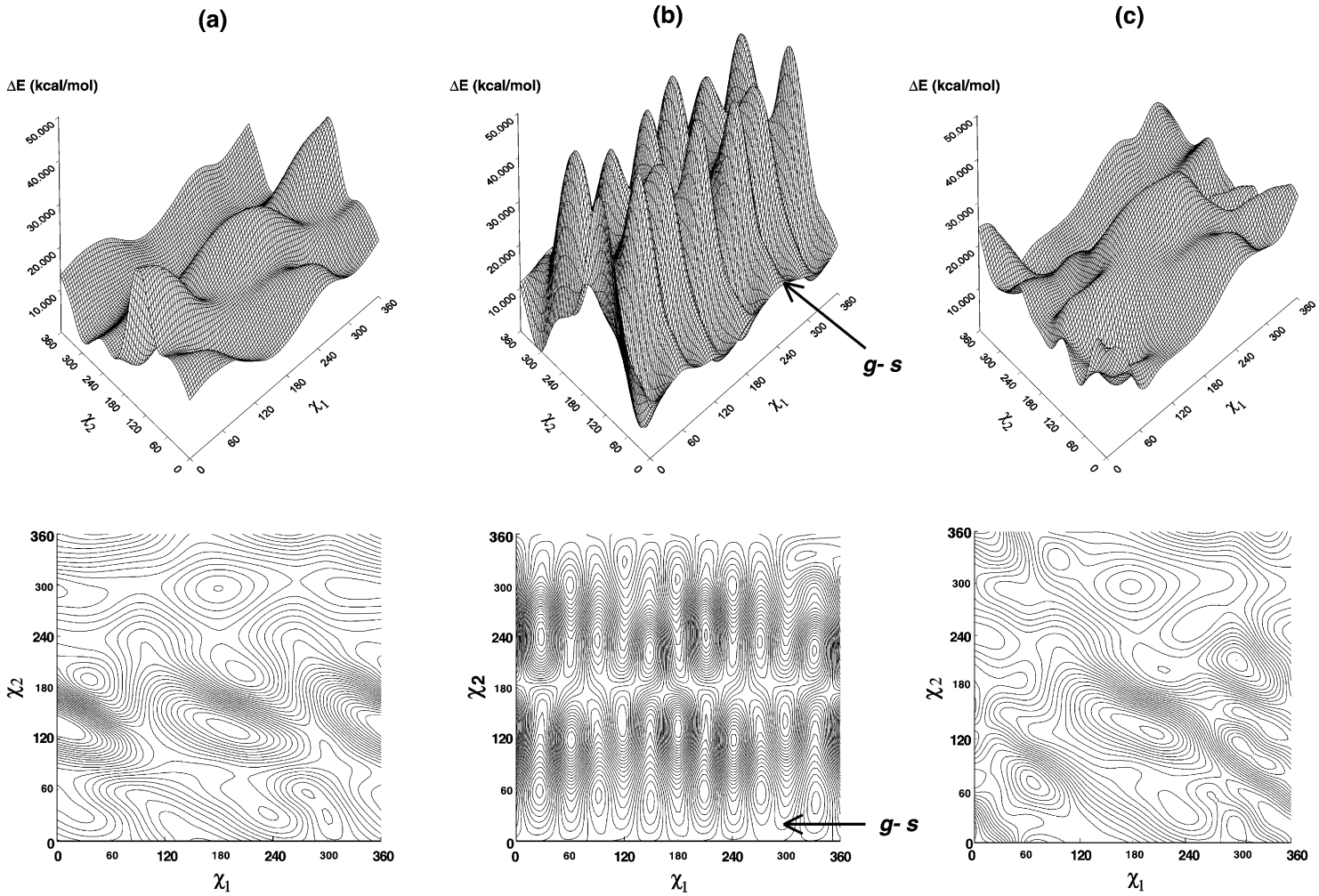

Fig. 11. Double-scan PES, $E = E(\chi_1, \chi_2)$, generated for the α_D backbone conformation of: (a) the *endo* form of *N*-acetyl-L-aspartic acid-*N*′-methylamide, (b) *N*-acetyl-L-aspartate-*N*′-methylamide, (c) the *exo* form of *N*-acetyl-L-aspartic acid-*N*′-methylamide in both landscape (top) and contour (bottom) representations. Note that the double-scan results for the *endo* and *exo* forms were previously published [1–2]. Torsional angles χ_1 and χ_2 are given in degrees.

Table 2
Geometric and energetic parameters of optimized conformers of *N*-acetyl-L-aspartic acid *N'*-methylamide in its *endo* form for all its stable backbone (γ_L, β_L, δ_L, α_L, γ_D, δ_D, α_D, and ε_D) conformation computed at the B3LYP/6-31G(d) level of theory. Shown here are the optimized torsional angles, computed energy values, relative energies, and stabilization energies

Final conform.	Optimized parameters									
BB [χ_1,χ_2]	χ_1	χ_2	ω_0	ω_1	ϕ	ψ	E_{min} (Hartree)	ΔE (kcal/mol)	ΔE^{stabil} (kcal) β_L	ΔE^{stabil} (kcal) γ_L
γ_L Backbone conformation										
γ_L [g^+s^+]	58.85	144.19	−179.63	−176.47	−82.63	69.39	−684.4260542	0.000	−7.5936	−6.4623
γ_L [g^+g^-]	67.76	−41.53	−179.64	−176.59	−83.22	70.88	−684.4210847	3.118	−4.4751	−3.3439
γ_L [$a\ s$]	−176.54	27.91	−178.12	−177.73	−83.13	69.16	−684.4178720	5.134	−2.4591	−1.3279
γ_L [$a\ a$]	−169.19	−163.60	−179.13	−177.93	−82.80	71.63	−684.4199177	3.851	−3.7428	−2.6116
γ_L g^-s^+]	−55.28	90.31	−173.51	−176.48	−83.30	71.37	−684.4190950	4.367	−3.2266	−2.0953
γ_L [g^-a]	−72.14	157.14	−173.78	−177.94	−84.30	66.13	−684.4189046	4.486	−3.1071	−1.9758
γ_L [g^-s^-]	−45.07	−119.39	−170.48	−175.81	−83.95	72.82	−684.4217674	2.690	−4.9035	−3.7723
β_L Backbone conformation										
β_L [g^+s^+]	58.82	107.24	−169.30	175.92	−170.22	150.84	−684.4154168	6.675	−0.9185	0.2128
β_L [g^+a][a,b]	66.22	−171.49	173.48	−179.57	−157.77	−177.22	−684.4153786	6.699	−0.8945	0.2368
β_L [a g^+]	−173.28	32.25	177.73	177.71	−164.40	162.84	−684.4184974	4.742	−2.8516	−1.7203
β_L [$a\ a$]	−161.48	173.27	175.07	178.61	−163.51	167.73	−684.4240236	1.274	−6.3193	−5.1881
δ_L Backbone conformation										
δ_L [g^+s]	69.12	−26.01	−170.39	176.65	−130.53	32.86	−684.4164380	6.034	−1.5593	−0.4280
δ_L [g^+a][a,b]	60.44	162.32	−170.27	177.91	−130.74	30.06	−684.4215144	2.849	−4.7448	−3.6135
δ_L [a g^+]	−172.91	37.96	−170.11	175.22	−135.53	34.83	−684.4130412	8.166	0.5722	1.7035
δ_L [g^-g^+]	−67.72	82.47	−164.18	174.86	−135.08	25.11	−684.4133097	7.997	0.4037	1.5350
δ_L [g^-s^-]	−56.89	−98.79	−161.57	175.51	−133.61	22.39	−684.4155795	6.573	−1.0206	0.1107
α_L Backbone conformation										
α_L [g^-s^-][a,b]	−55.35	−119.10	−164.10	176.83	−81.20	−13.35	−684.4153827	6.696	−0.8971	0.2342
γ_D Backbone conformation										
γ_D [a g^+]	−170.77	65.87	175.99	−176.30	73.01	−53.01	−684.4128945	8.258	0.6643	1.7956
γ_D [a s^-][a,b]	−155.29	−145.77	178.99	177.75	74.54	−65.87	−684.4128963	8.257	0.6632	1.7944
γ_D [g^-a]	−64.89	179.52	168.25	−178.12	73.63	−49.71	−684.4181554	4.957	−2.6370	−1.5057
γ_D [g^-g^-]	−59.41	−37.44	172.24	−178.73	72.81	−53.52	−684.4146876	7.133	−0.4609	0.6704
δ_D Backbone conformation										
δ_D [g^+g^+][a,b]	43.03	44.58	171.16	−175.78	−155.89	−38.80	−684.4069299	12.001	4.4071	5.5384
δ_D [g^+a][a,b]	54.07	−168.35	174.77	−176.77	−156.90	−48.59	−684.4146306	7.168	−0.4251	0.7061
δ_D [g^+g^-]	67.67	−35.23	176.01	−175.35	−164.26	−45.65	−684.4075771	11.595	4.0010	5.1323
δ_D [a g^+]	178.57	65.29	168.72	−171.72	−169.53	−39.89	−684.4067348	12.123	4.5296	5.6608
δ_D [a s^-]	−172.30	−117.79	167.19	−172.40	−173.40	−36.11	−684.4058219	12.696	5.1024	6.2337
δ_D [g^-g^-][a,b]	−61.73	−79.40	178.05	−176.94	−144.09	−61.07	−684.4052097	13.080	5.4866	6.6178
α_D Backbone conformation										
α_D [g^+s^+]	42.53	102.03	161.69	−175.78	58.20	35.63	−684.4070563	11.921	4.3278	5.4591
α_D [g^+g^-]	55.10	−81.81	164.08	−176.20	59.50	29.35	−684.4040903	13.783	6.1890	7.3203
α_D [a g^+]	−167.04	37.82	168.69	−176.91	65.49	31.81	−684.4097827	10.211	2.6170	3.7482
α_D [a s^-]	−157.47	−149.78	169.86	−177.78	66.30	32.61	−684.4122840	8.641	1.0474	2.1787
α_D [g^-s]	−63.19	−18.36	166.07	−177.25	66.36	28.71	−684.4119363	8.859	1.2656	2.3968
α_D [g^-a]	−64.43	−176.83	164.61	−177.19	66.01	30.43	−684.4166005	5.932	−1.6613	−0.5300
ε_D Backbone conformation										
ε_D [g^+g^+]	51.08	89.57	−176.20	177.24	53.92	−123.45	−684.4079873	11.337	3.7436	4.8749
ε_D [g^+s^-]	69.41	−103.68	−164.86	179.14	57.16	−134.18	−684.4113997	9.196	1.6023	2.7336
ε_D [s^-a]	−149.86	160.48	−158.02	−175.88	66.93	−178.82	−684.4142905	7.382	−0.2117	0.9196
ε_D [s^-g^-]	−135.38	−50.94	−160.60	−175.48	64.41	−167.41	−684.4076898	11.524	3.9303	5.0616

Note: The information presented in this table has been published before [2]. The numerical values are presented here for the sake of comparison with the optimized results for *N*-acetyl-L-aspartate-*N'*-methylamide.

[a] After 200 iterations under B3LYP/6-31G(d) at (TIGHT, Z-MATRIX), the force has converged, but the displacement did not converge completely.

[b] This result was obtained from an optimization fully converged under regular B3LYP/6-31G(d) at (Z-MATRIX).

Table 3
Geometric and energetic parameters of optimized conformers of *N*-acetyl-L-aspartic acid *N'*-methylamide in its *exo* form for all its stable backbone (γ_L, β_L, δ_L, ε_L, γ_D, δ_D, α_D, and ε_D) conformation computed at the B3LYP/6-31G(d) level of theory. Shown here are the optimized torsional angles, computed energy values, relative energies, and stabilization energies

Final Conform.	Optimized parameters										
BB [χ_1,χ_2]	χ_1	χ_2	χ_3	ϕ	ψ	ω_0	ω_1	E_{min} (Hartree)	ΔE (kcal/mol)	ΔE^{stabil} (kcal) β_L	ΔE^{stabil} (kcal) γ_L
γ_L Backbone conformation											
γ_L [g^+g^+]	50.73	82.28	−13.95	−81.06	63.58	−171.12	−179.73	−684.4265160	−0.290	−13.7932	−12.6619
γ_L [g^+g^+]	50.58	82.31	−13.98	−81.91	63.80	−170.70	−179.40	−684.4266579	−0.379	−13.8822	−12.7509
γ_L [$a\ g^-$]	−165.32	−70.57	4.41	−83.16	64.17	−172.10	−179.20	−684.4208809	3.246	−10.2571	−9.1258
γ_L [g^-s^-]	−45.91	−121.27	0.59	−84.07	70.53	−169.26	−176.36	−684.4126227	8.428	−5.0750	−3.9437
β_L Backbone conformation											
β_L [g^+g^+][a,b]	64.56	72.14	−1.65	−156.59	−176.43	177.82	−171.12	−684.4058456	12.681	−0.8223	0.3090
β_L [g^+s^-]	63.71	−90.93	6.92	158.11	−139.74	172.36	179.88	−684.4201077	3.731	−9.7719	−8.6406
β_L [$a\ a$]	−159.70	167.29	−3.78	−167.29	170.92	174.39	179.24	−684.4161709	6.202	−7.3015	−6.1702
β_L [s^-g^+]	−130.05	74.37	−4.45	−169.92	−177.45	175.01	−179.22	−684.4237651	1.436	−12.0669	−10.9357
δ_L Backbone conformation											
δ_L [s^-g^+][a,b]	−118.31	48.09	4.66	−161.43	45.11	−176.35	173.71	−684.4099383	10.113	−3.3905	−2.2592
δ_L [g^-s]	−67.01	−15.76	14.84	−135.40	25.16	−177.58	174.07	−684.4103060	9.882	−3.6212	−2.4900
ε_L Backbone conformation											
ε_L [g^-g^+]	−63.25	43.99	−5.09	−94.47	149.36	160.78	177.79	−684.4102974	9.888	−3.6158	−2.4846
γ_D Backbone conformation											
γ_D [g^+g^+]	60.23	67.68	−17.12	64.96	−61.81	168.52	175.34	−684.4033200	14.266	0.7625	1.8938
γ_D [s^+g^-]	107.66	−75.40	6.66	79.72	−53.75	−177.65	−174.22	−684.4073279	11.751	−1.7524	−0.6212
γ_D [$a\ a$]	−154.73	−154.72	4.80	74.38	−70.80	−179.62	175.29	−684.4035338	14.132	0.6284	1.7597
γ_D [a g^-]	−176.52	−70.85	4.12	70.34	−81.17	177.02	172.78	−684.4078146	11.446	−2.0579	−0.9266
γ_D [s^-g^-]	−143.16	−35.94	−3.53	70.12	−28.28	167.77	−175.15	−684.4144381	7.289	−6.2142	−5.0829
γ_D [g^-a]	−63.68	176.48	−0.54	73.63	−44.57	167.30	−177.58	−684.4098022	10.198	−3.3051	−2.1738
δ_D Backbone conformation											
δ_D [g^+a][a,b]	52.48	−164.30	3.41	−160.74	−48.85	175.72	−176.93	−684.4071457	11.865	−1.6381	−0.5068
δ_D [g^+g^-][a,b]	62.86	−42.90	−3.04	−152.24	−46.34	162.79	−174.56	−684.4046175	13.452	−0.0516	1.0796
δ_D [s^-g^+]	−121.06	55.27	4.53	−166.96	−52.06	172.53	−173.85	−684.4070418	11.930	−1.5729	−0.4416
δ_D [g^-s][a,b]	−79.12	2.05	12.10	−135.56	−70.97	168.84	−177.26	−684.4055002	12.898	−0.6055	0.5257
α_D Backbone conformation											
α_D [g^+g^+]	57.95	78.07	−13.34	51.02	50.87	158.65	−173.41	−684.4118612	8.906	−4.5971	−3.4659
α_D [g^+g^-]	42.68	−69.95	7.37	49.91	35.67	175.22	−176.17	−684.3904410	22.348	8.8442	9.9755
α_D [s^-g^-]	−147.48	−61.61	0.62	68.57	27.90	165.45	−178.48	−684.4145135	7.242	−6.2615	−5.1302
α_D [g^-a]	−64.08	−177.94	0.92	66.58	30.54	164.64	−177.60	−684.4094323	10.430	−3.0730	−1.9417
ε_D Backbone conformation											
ε_D [$a\ a$]	−152.00	171.32	−0.35	68.83	176.68	−157.00	−176.55	−684.4069842	11.967	−1.5368	−0.4055
ε_D [g^-g^+]	−62.34	93.43	−7.44	85.36	163.60	−152.58	178.97	−684.4096079	10.320	−3.1832	−2.0519

Note: The information presented in this table has been published before [1]. The numerical values are presented here for the sake of comparison with the optimized results for *N*-acetyl-L-aspartate-*N'*-methylamide.

[a] After 200 iterations under B3LYP/6-31G(d) at (TIGHT, Z-MATRIX), the force has converged, but the displacement did not converge completely.

[b] This result was obtained from an optimization fully converged under regular B3LYP/6-31G(d) at (Z-MATRIX).

the aspartic acid residue at B3LYP/6-31G(d) compared to the seven stable structures found for the aspartate. Tables 2 and 3 show the optimized parameters of the stable conformers found for the *endo* and *exo* forms of *N*-acetyl-L-aspartic acid-*N*′-methylamide. Clearly, the number of stable conformers found in both *endo* and *exo* forms of *N*-acetyl-L-aspartic acid-*N*′-methylamide far exceed those found in *N*-acetyl-L-aspartate-*N*′-methylamide, suggesting that the complexity of the protonation pattern for the aspartate residue far exceeds the initial hypothesis. Comparing the energy (E_{min}) of the conformers found for the aspartate residue against those found for the aspartic acid residue provide some clues to explain the dilemma concerning the aspartate protonation pattern (Tables 4–7). From Tables 4–7, it is shown that the energy difference between aspartate conformers and aspartic acid conformers is approximately 340 kcal/mol (or 0.54 Hartree). This means that protonating the aspartate residue may stabilize the overall geometry of each conformer optimized, since the pronated aspartic acid has lower energies than the deprotonated aspartate. More noticeably, however, is the difference between the stabilization energy exerted

Table 4
Deprotonation energies found for the *endo* and *exo* conformers of *N*-acetyl-L-aspartic acid-*N*′-methylamide against conformers optimized for *N*-acetyl-L-aspartate-*N*′-methylamide in the γ_L backbone conformation at the B3LYP/6-31G(d) level of theory

Aspartate	E_{min} (Hartree)	Aspartic acid *endo*	E_{min} (Hartree)	vs γ_L [g^+s] (Hartree)	vs γ_L [g^+s] ΔE (kcal/mol)	vs γ_L [g^-g^+] (Hartree)	vs γ_L [g^-g^+] ΔE (kcal/mol)
γ_L [g^+s]	−683.8711687	γ_L [g^+s^+]	−684.4260542	0.5549	348.1959	0.5528	346.8964
γ_L [g^-g^+]	−683.8732396	γ_L [g^+g^-]	−684.4210847	0.5549	348.1959	0.5478	343.7780
		γ_L [$a\ s$]	−684.4178720	0.5499	345.0775	0.5446	341.7620
		γ_L [$a\ a$]	−684.4199177	0.5487	344.3452	0.5467	343.0457
		γ_L [g^-s^+]	−684.4190950	0.5479	343.8290	0.5459	342.5294
		γ_L [$g^-\ a$]	−684.4189046	0.5477	343.7095	0.5457	342.4100
		γ_L [g^-s^-]	−684.4217674	0.5506	345.5059	0.5485	344.2064
		Aspartic acid *exo*					
		γ_L [g^+g^+]	−684.4265160	0.5553	348.4857	0.5533	347.1862
		γ_L [g^+g^+]	−684.4266579	0.5555	348.5748	0.5534	347.2752
		γ_L [$a\ g^-$]	−684.4208809	0.5497	344.9496	0.5476	343.6501
		g_L [g^-s^-]	−684.4126227	0.5415	339.7675	0.5394	338.4680

Note that the relative energies for both *endo* and *exo* forms of *N*-acetyl-L-aspartic acid-*N*′-methylamide were previously published [1,2].

Table 5
Deprotonation energies found for the *endo* and *exo* conformers of *N*-acetyl-L-aspartic acid-*N*′-methylamide against conformers optimized for *N*-acetyl-L-aspartate-*N*′-methylamide in the β_L backbone conformation at the B3LYP/6-31G(d) level of theory

Aspartate	E_{min} (Hartree)	Aspartic acid *endo*	E_{min} (Hartree)	vs β_L [$a\ s$] (Hartree)	vs β_L [$a\ s$] ΔE (kcal/mol)
β_L [$a\ s$]	−683.8760086	β_L [g^+s^+]	−684.4154168	0.5394	338.4838
		β_L [g^+a][a,b]	−684.4153786	0.5394	338.4598
		β_L [ag^+]	−684.4184974	0.5425	340.4169
		β_L [$a\ a$]	−684.4240236	0.5480	343.8846
		Aspartic acid *exo*			
		β_L [g^+g^+][a,b]	−684.4058456	0.5298	332.4778
		β_L [g^+s^-]	−684.4201077	0.5441	341.4274
		β_L [$a\ a$]	−684.4161709	0.5402	338.9570
		β_L [s^-g^+]	−684.4237651	0.5478	343.7224

Note that the relative energies for both *endo* and *exo* forms of *N*-acetyl-L-aspartic acid-*N*′-methylamide were previously published [1,2].

[a] After 200 iterations under B3LYP/6-31G(d) at (TIGHT, Z-MATRIX), the force has converged, but the displacement did not converge completely.

[b] This result was obtained from an optimization fully converged under regular B3LYP/6-31G(d) at (Z-MATRIX).

Table 6
Deprotonation energies found for the *endo* and *exo* conformers of *N*-acetyl-L-aspartic acid-*N*′-methylamide against conformers optimized for *N*-acetyl-L-aspartate-*N*′-methylamide in the α_L backbone conformation at the B3LYP/6-31G(d) level of theory

Aspartate	E_{min} (Hartree)	Aspartic acid *endo*	E_{min} (Hartree)	vs α_L [g^+s^+] (Hartree)	vs α_L [g^+s^+] ΔE (kcal/mol)	vs α_L [g^+s] (Hartree)	vs α_L [g^+s] Δ_E (kcal/mol)	vs α_L [g^-g^+] (Hartree)	vs α_L [g^-g^+] ΔE (kcal/mol)
α_L [g^+s^+]	−683.8755999	α_L [g^-s^-][a,b]	−684.4153827	0.5398	338.7188	0.5355	336.0586	0.5455	342.3126
α_L [g^+s]	−683.8798393	Aspartic acid *exo*							
α_L [g^-g^+]	−683.8698728	–	–	–	–	–	–	–	–

Note that the relative energies for the *endo* form of *N*-acetyl-L-aspartic acid-*N*′-methylamide were previously published [1,2]. No stable conformer for the *exo* form of *N*-acetyl-L-aspartic acid-*N*′-methylamide could be found.
[a] After 200 iterations under B3LYP/6-31G(d) at (TIGHT, Z-MATRIX), the force has converged, but the displacement did not converge completely.
[b] This result was obtained from an optimization fully converged under regular B3LYP/6-31G(d) at (Z-MATRIX).

by the sidechain on the backbone for the aspartate and aspartic acid residues (Tables 1–3). When comparing the stabilization energy values between Tables 1–3, it is clear that the aspartate sidechain, while losing its proton, can stabilize its backbone geometry in a greater extend than the aspartic acid sidechain. If this is the case, then it suggests that when deprotonated, the lone electron in the negatively charged aspartate sidechain allows for greater stabilization effects on its backbone than the aspartic acid sidechain. In this scenario, both r[C−O] and R[C−O*] may participate in hydrogen bond interactions with the backbone atoms and stabilizing the backbone geometry.

When protonating the aspartate residue, there are more geometric choices by which the proton can dock itself (Fig. 12). As shown in Fig. 12, there are, in general, more *endo* and *exo* conformers of the aspartic acid residue surrounding the aspartate conformers in most backbone conformations. Interestingly, however, there are three aspartate conformers found for the α_L backbone conformation while only one stable conformer was found in both *endo* and *exo* forms of the aspartic acid (Fig. 12(b)). This finding may suggest that a particular aspartic acid conformer might need to change its backbone conformation before it can be deprotonated into a stable aspartate form.

Fig. 13 shows the traditional hydrogen interactions that may exist in *N*-acetyl-L-aspartate-*N*′-methylamide. The various types of hydrogen bond interactions were tabulated in Table 8. There were two backbone–backbone (BB/BB) and four backbone–sidechain (BB/SC) interactions. Although hydrogen bonding represents only weak interactions in inter- and intra-molecular structures, their presence is still significant and especially in ligand binding and protein–ligand recognitions. If the aspartyl residue was coded in a receptor or an ion channel, BB/BB interactions may help stabilize the aspartyl residue in a peptide chain, BB/SC interactions would allow for ligand binding and recognition by forming an overall stable structure with the ligand. In addition, since the aspartyl residue is involved in the RGD tripeptide, these hydrogen bond interactions may be significant in peptide folding, where both BB/BB and BB/SC interactions might be important in forming stabilized structures. The aspartate sidechain stabilizes the backbone more than its protonated form. As shown

Table 7
Deprotonation energies found for the *endo* and *exo* conformers of *N*-acetyl-L-aspartic acid-*N'*-methylamide against conformers optimized for *N*-acetyl-L-aspartate-*N'*-methylamide in the α_D backbone conformation at the B3LYP/6-31G(d) level of theory

Aspartate	E_{min} (Hartree)	Aspartic acid *endo*	E_{min} (Hartree)	vs α_D [g^-s] (Hartree)	vs α_D [g^-s] ΔE (kcal/mol)
α_D [g^-s]	−683.8613062	α_D [g^+s^+]	−684.4070563	0.5458	342.4634
		α_D [g^+g^-]	−684.4040903	0.5428	340.6022
		α_D [a g^+]	−684.4097827	0.5485	344.1742
		α_D [a s^-]	−684.4122840	0.5510	345.7438
		α_D [g^-s]	−684.4119363	0.5506	345.5256
		α_D [g^-a]	−684.4166005	0.5553	348.4524
		Aspartic acid *exo*			
		α_D [g^+g^+]	−684.4118612	0.5506	345.4785
		α_D [g^+g^-]	−684.3904410	0.5291	332.0371
		α_D [s^-g^-]	−684.4145135	0.5532	347.1428
		α_D [g^-a]	−684.4094323	0.5481	343.9543

Note that the relative energies for both endo and exo forms of *N*-acetyl-L-aspartic acid-*N'*-methylamide were previously published [1,2].

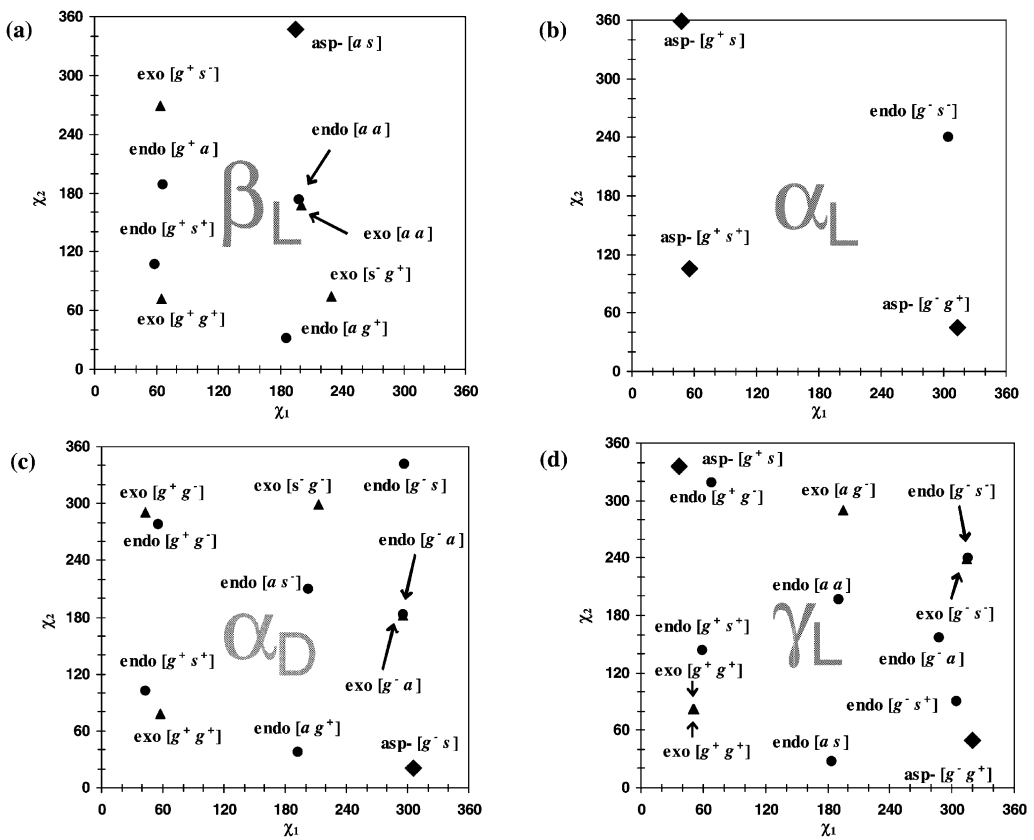

Fig. 12. Scatter-plot diagrams showing the optimized conformers found for *N*-acetyl-L-aspartate-*N'*-methylamide and the *endo* and *exo* forms of *N*-acetyl-L-aspartic acid-*N'*-methylamide in the (a) β_L, (b) α_L, (c) α_D, and (d) γ_L backbone conformations. Note: rhombus represents *N*-acetyl-L-aspartate-*N'*-methylamide, circle represents the *endo* form of *N*-acetyl-L-aspartic acid-*N'*-methylamide, and triangles represent the *exo* form of *N*-acetyl-L-aspartic acid-*N'*-methylamide.

Backbone-Backbone Interactions
(BB/BB)

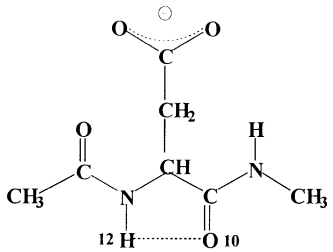

Intramolecular H-bonded
Interaction Type: **1A**
Distance: O^{10}·····H^{12}
Ring Size: 5

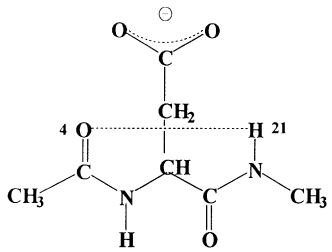

Intramolecular H-bonded
Interaction Type: **1B**
Distance: O^{4}·····H^{21}
Ring Size: 7

Backbone-Sidechain Interactions
(BB/SC)

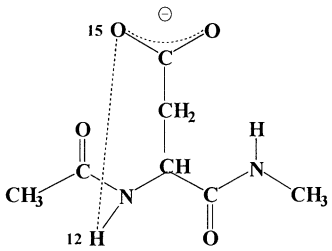

Intramolecular H-bonded
Interaction Type: **2A**
Distance: H^{12}·····O^{15}
Ring Size: 6

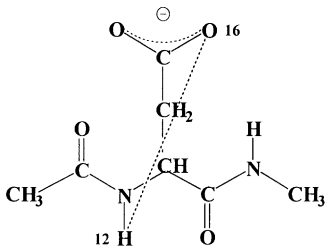

Intramolecular H-bonded
Interaction Type: **2B**
Distance: H^{12}·····O^{16}
Ring Size: 6

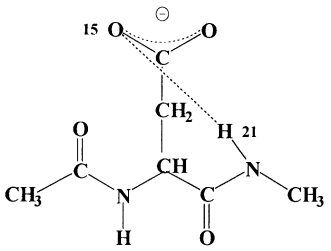

Intramolecular H-bonded
Interaction Type: **2C**
Distance: O^{15}·····H^{21}
Ring Size: 6

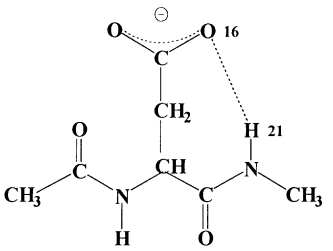

Intramolecular H-bonded
Interaction Type: **2D**
Distance: O^{16}·····H^{21}
Ring Size: 6

Fig. 13. Classification of the 'traditional' hydrogen bond interactions for *N*-acetyl-L-aspartate-*N'*-methylamide.

Table 8
The relative distances of potential hydrogen bonds of *N*-acetyl-L-aspartate-*N*′-methylamide for all its stable backbone (γ_L, β_L, α_L, and α_D) conformations computed at the B3LYP/6-31G(d) level of theory. No conformers were found for the δ_L, ε_L, γ_D, δ_D, and ε_D backbone conformations and hence no hydrogen bond distances for these backbones could be tabulated

Final conform.	Interaction type		Distance (Å)					
BB [$\chi_1\chi_2$]	BB/BB	SC/BB	H12–O10	H12–O15	H12–O16	H21–O4	H21–O15	H21–O16
γ_L [g^+s]	1B	2A	3.782	1.561	3.484	1.896	4.894	6.074
γ_L [g^-g^+]	1B	2A	3.982	1.583	3.441	1.844	5.171	6.060
β_L [a s]	1A	2C	2.021	4.926	5.530	5.129	1.601	3.524
α_L [g^+s^+]	–	2B, 2C	3.734	3.489	1.912	5.439	1.832	3.278
α_L [g^+s]	–	2A, 2C	4.066	1.899	3.643	4.764	1.802	3.552
α_L [g^-g^+]	–	2A	4.417	1.632	3.518	3.082	4.331	5.558
α_D [g^-s]	–	2A	4.368	1.693	3.633	2.721	4.810	6.142

in Table 8, all stable conformers of the aspartate residue have at least one type of hydrogen bond interaction. Because it is an anion, the aspartate sidechain may participate in more hydrogen bond interactions than the aspartic acid sidechain; and each atom in the aspartate molecule will repel against one another to a greater extend than in the aspartic acid residue. Clearly, this situation will cause the overall bond length to be somewhat longer in the aspartate than in the aspartic acid, resulting in higher energies for the aspartate conformers.

By subtracting the PEHSs of the *endo* and *exo* forms of *N*-acetyl-L-aspartic acid-*N*′-methylamide from that of *N*-acetyl-L-aspartate-*N*′-methylamide in their respective backbone conformations (γ_L, β_L, α_L, α_D), the vertical deprotonation PEHS of *N*-acetyl-L-aspartic acid-*N*′-methylamide can be found (Fig. 14–17). In general, the deprotonation patterns of both *endo* and *exo* forms of *N*-acetyl-L-aspartic acid-*N*′-methylamide were similar, where the PEHSs show similar minima and maxima. The greatest difference in deprotonation patterns for both the *endo* and *exo* forms of the aspartic acid residue was shown in the β_L backbone conformation (Fig. 15(a) and (c)).

In closing, it should be emphasized that aspartate sidechain surfaces were possible to compute for the γ_L, β_L, α_L and α_D backbone conformations. However, such surfaces could not be generated for the remaining five backbone conformations. All attempts failed because many of the points were considerably higher (data not shown) than the normal deprotonation energy. For this reason it seems that the aspartic acid residue would rather change conformation to the favorable backbone structures (γ_L, β_L, α_L, α_D) before it would undergo deprotonation. In this case, a conformer of the aspartic acid residue in the δ_L, ε_L, γ_D, δ_D, and ε_D backbone conformations (where no stable conformers could be found for the aspartate residue) would migrate to its nearest neighbors (γ_L, β_L, α_L, or α_D) by changing either the ϕ or the ψ torsional angles. These 'nearest neighbors' also represent the 'allowed' backbone conformations where stable conformers of aspartate residue were found (γ_L, β_L, α_L, and α_D). This model is shown in Fig. 18, where there are three backbone conformations (γ_D, δ_D, and ε_D) with two nearest allowed neighbors and two backbone conformations (δ_L and ε_L) with three nearest allowed neighbors.

4. Conclusions

Only seven of the initially expected 81 conformers were found for *N*-acetyl-L-aspartate-*N*′-methylamide at the B3LYP/6-31G(d) level of theory. These stable conformers were located at the γ_L, β_L, α_L, and α_D backbone conformations while no conformers could be found in the δ_L, ε_L, γ_D, δ_D, and ε_D backbones. By comparing the relative energies of the *endo* and *exo* forms of *N*-acetyl-L-aspartic acid-*N*′-methylamide against those of *N*-acetyl-L-aspartate-*N*′-methylamide, the adiabatic deprotonation energies for the aspartic acid residue were found. The deprotonation patterns of the *endo* and *exo* forms of *N*-acetyl-L-aspartic

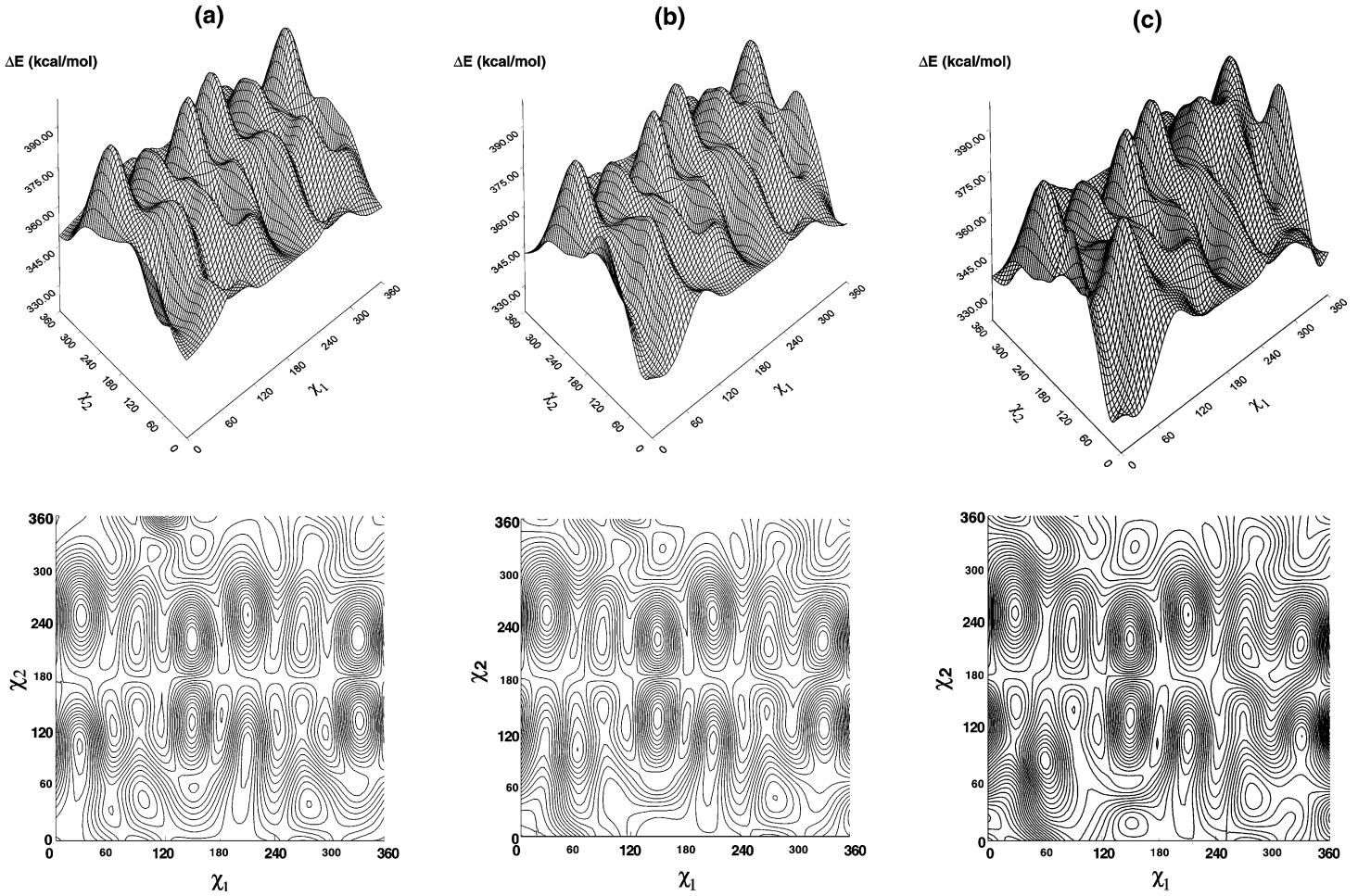

Fig. 14. Double-scan PES, $E = E(\chi_1, \chi_2)$, generated for the deprotonation energies of (a) the *endo*, (b) the average deprotonation energies of both *endo* and *exo* forms, and (c) the *exo* forms of *N*-acetyl-L-aspartic acid-*N*′-methylamide in its γ_L backbone conformation. Torsional angles χ_1 and χ_2 are given in degrees.

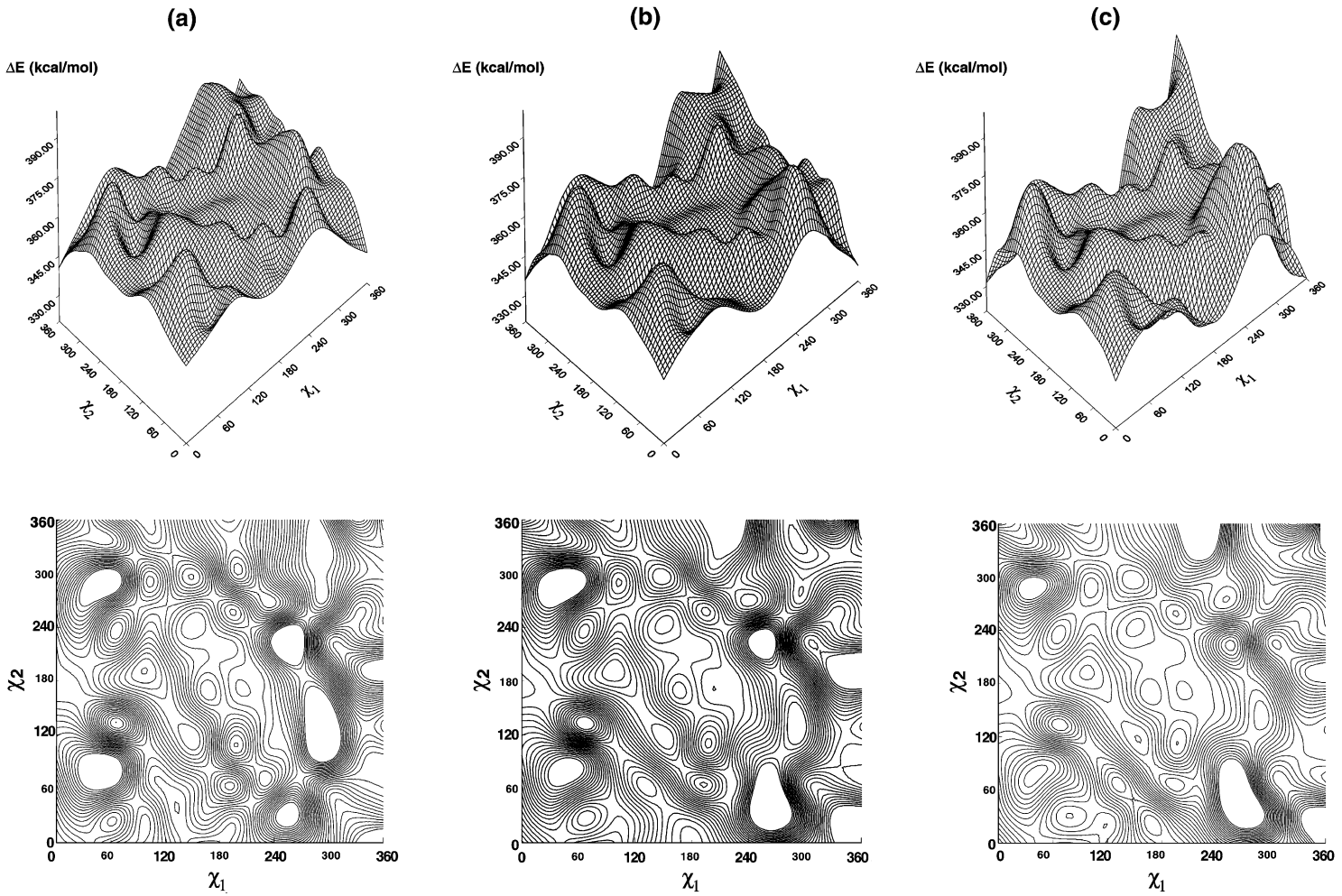

Fig. 15. Double-scan PES, $E = E(\chi_1, \chi_2)$, generated for the deprotonation energies of (a) the *endo*, (b) the average deprotonation energies of both *endo* and *exo* forms, and (c) the *exo* forms of *N*-acetyl-L-aspartic acid-N'-methylamide in its β_L backbone conformation. Torsional angles χ_1 and χ_2 are given in degrees.

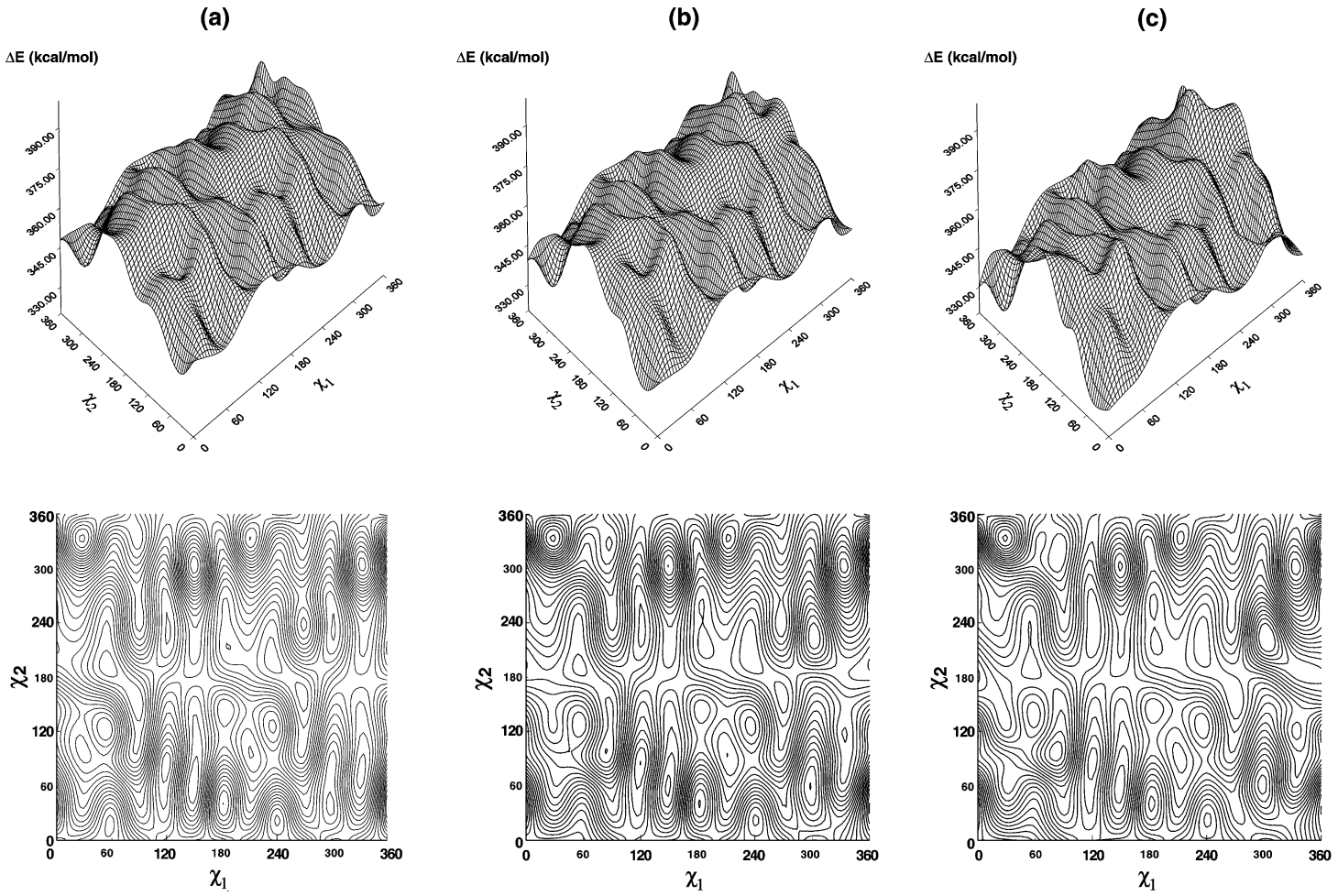

Fig. 16. Double-scan PES, $E = E(\chi_1, \chi_2)$, generated for the deprotonation energies of (a) the *endo*, (b) the average deprotonation energies of both *endo* and *exo* forms, and (c) the *exo* forms of *N*-acetyl-L-aspartic acid-*N*′-methylamide in its α_L backbone conformation. Torsional angles χ_1 and χ_2 are given in degrees.

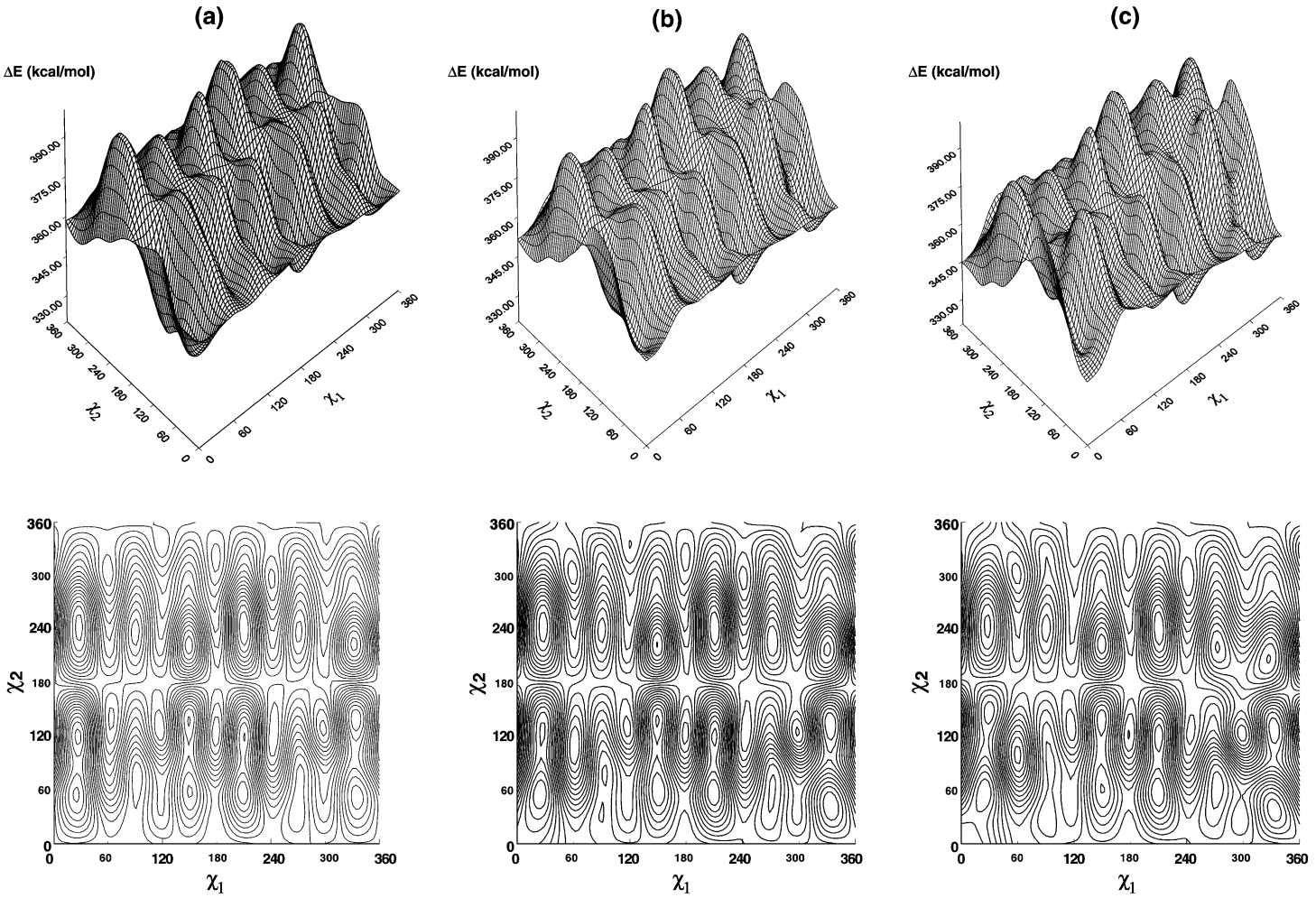

Fig. 17. Double-scan PES, $E = E(\chi_1, \chi_2)$, generated for the deprotonation energies of (a) the *endo*, (b) the average deprotonation energies of both *endo* and *exo* forms, and (c) the *exo* forms of *N*-acetyl-L-aspartic acid-*N*′-methylamide in its α_D backbone conformation. Torsional angles χ_1 and χ_2 are given in degrees.

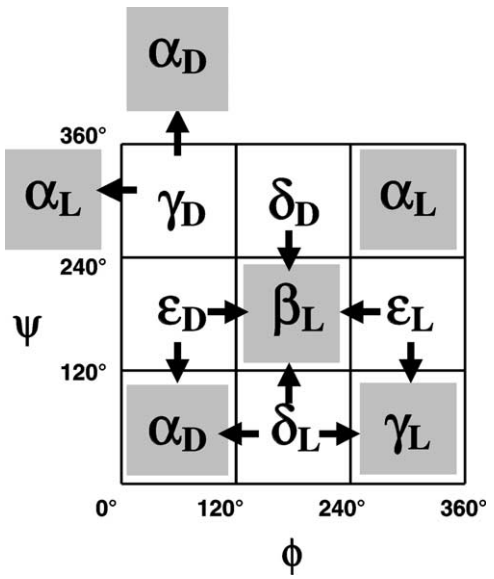

Fig. 18. A schematic representation of the backbone conformational change of aspartic acid residue prior to sidechain deprotonation to the corresponding aspartate residue.

acid-*N*′-methylamide with respect to *N*-acetyl-L-aspartate-*N*′-methylamide were established. The sidechain PEHSs for the vertical deprotonation energies of the *endo* and *exo* forms of *N*-acetyl-L-aspartate-*N*′-methylamide showed similarities as well as difference in the deprotonation patterns between the two forms. Two types of hydrogen bond interactions were found for *N*-acetyl-L-aspartate-*N*′-methylamide: backbone–sidechain (N–H···$^{-}$O–C) and backbone–backbone (N–H···O=C). In sum, there were a total of two backbone–backbone and four backbone–sidechain interactions for the aspartate residue. In addition, these hydrogen bond interactions may help explain the geometric preference of RGD during peptide folding as well as the importance of the aspartyl residue during such molecular processes as ligand binding and ligand recognition by cell receptors.

Acknowledgements

The authors would like to express their gratitude for the generous allocation of CPU time provided by the National Cancer Institute (NCI) at the Frederick Biomedical Supercomputing Center.

References

[1] J.C.P. Koo, G.A. Chass, A. Perczel, Ö. Farkas, L.L. Torday, A. Varro, J.G. Papp, I.G. Csizmadia, Eur. Phys. J. D (2002) in press.
[2] J.C.P. Koo, G.A. Chass, A. Perczel, Ö. Farkas, L.L. Torday, A. Varro, J.G. Papp, I.G. Csizmadia, J. Phys. Chem. A 106 (2002) 6999.
[3] A. Percel, J.G. Ángyán, M. Kajtár, W. Viviani, J.L. Rivail, J.F. Marcoccia, I.G. Csizmadia, J. Am. Chem. Soc. 113 (1991) 6256.
[4] M.A. McAllister, A. Perczel, P. Császár, W. Viviani, J.L. Rivail, I.G. Csizmadia, J. Mol. Struct. (Theochem) 288 (1993) 161.
[5] M.A. McAllister, A. Perczel, P. Császár, I.G. Csizmadia, J. Mol. Struct. (Theochem) 288 (1993) 181.
[6] A. Perczel, M.A. McAllister, P. Császár, I.G. Csizmadia, Can. J. Chem. 72 (1994) 2050.
[7] M. Cheung, M.E. McGovern, T. Jin, D.C. Zhao, M.A. McAllister, A. Perczel, P. Császár, I.G. Csizmadia, J. Mol. Struct. (Theochem) 309 (1994) 151.
[8] A.M. Rodriguez, H.A. Baldoni, F. Suvire, R. Nieto-Vasquez, G. Zamarbide, R.D. Enriz, Ö. Farkas, A. Perczel, I.G. Csizmadia, J. Mol. Struct. (Theochem) 455 (1998) 275.
[9] M. Berg, S.J. Salpietro, A. Perczel, Ö. Farkas, I.G. Csizmadia, J. Mol. Struct. (Theochem) 504 (2000) 127.
[10] M.A. Zamora, H.A. Baldoni, J.A. Bombasaro, M.L. Mak, A. Perczel, Ö. Farkas, R.D. Enriz, J. Mol. Struct. (Theochem) 540 (2001) 271.
[11] M.A. Zamora, H.A. Baldoni, A.M. Rodriguez, R.D. Enriz, C.P. Sosa, A. Perczel, A. Kucsman, O. Farkas, E. Deretey, J.C. Vank, I.G. Csizmadia, Can. J. Chem. 80 (2002) 832.
[12] A. Perczel, Ö. Farkas, I.G. Csizmadia, J. Am. Chem. Soc. 117 (1995) 1653.
[13] H.A. Baldoni, G.N. Zamarbide, R.D. Enriz, E.A. Jauregui, Ö. Farkas, A. Perczel, S.J. Salpietro, I.G. Csizmadia, J. Mol. Struct. (Millennium Volume) 500 (2000) 97.
[14] Ö. Farkas, M.A. McAllister, J.H. Ma, A. Perczel, M. Hollósi, I.G. Csizmadia, 369 (1996) 105.
[15] A. Perczel, Ö. Farkas, I.G. Csizmadia, Can. J. Chem. 75 (1997) 1120.
[16] I. Jakli, A. Perczel, Ö. Farkas, M. Hollosi, I.G. Csizmadia, J. Mol. Struct. (Theochem) 455 (1998) 303.
[17] H.A. Baldoni, A.M. Rodriguez, G. Zamarbide, R.D. Enriz, Ö. Farkas, P. Csaszar, L.L. Torday, C.P. Sosa, I. Jakli, A. Perczel, M. Hollosi, I.G. Csizmadia, J. Mol. Struct. (Theochem) 465 (1999) 79.
[18] J.C. Vank, C.P. Sosa, A. Perczel, I.G. Csizmadia, Can. J. Chem. 78 (2000) 395.
[19] A. Perczel, Ö. Farkas, I.G. Csizmadia, J. Comput. Chem. 17 (1996) 821.
[20] A. Perczel, Ö. Farkas, I.G. Csizmadia, J. Am. Chem. Soc. 118 (1996) 7809.
[21] I. Jakli, A. Perczel, Ö. Farkas, C.P. Sosa, I.G. Csizmadia, J. Comput. Chem. 21 (2000) 626.
[22] W. Viviani, J.-L. Rivail, A. Perczel, I.G. Csizmadia, J. Am. Chem. Soc. 115 (1993) 8321.

[23] D. Boehning, D.O. Mak, J.K. Foskett, S.K. Joseph, J. Biol. Chem. 276 (2001) 13509.
[24] D.W. Shin, J. Ma, D.H. Kim, FEBS Lett. 486 (2000) 178.
[25] B. Nilius, R. Vennekens, J. Prenen, J.G. Hoenderop, G. Droogmans, R.J. Bindels, J. Biol. Chem. 276 (2001) 1020.
[26] S. Hatse, K. Princen, L.O. Gerlach, G. Bridger, G. Henson, E. De Clercq, T.W. Schwartz, D. Schols, Mol. Pharmacol. 60 (2001) 164.
[27] G.F. Short III, A.L. Laikhter, M. Lodder, Y. Shayo, T. Arslan, S.M. Hecht, Biochemistry 39 (2000) 8768.
[28] J. Rotonda, M. Garcia-Calvo, H.G. Bull, W.M. Geissler, B. McKeever, N.A. Thornberry, J.W. Becker, Chem. Biol. 8 (2001) 357.
[29] K. Chlebovská, O. Chlebovskú, Mech. Ageing Dev. 108 (1999) 127.
[30] P. Fedoročko, N.O. Macková, Z. Šándorčínová-Hoferová, Z. Sedláková-Hoferová, P. Solár, O. Chlebovskú, Mech. Ageing Dev. 119 (2000) 159.
[31] C. Demougeot, P. Garnier, C. Mossiat, N. Bertrand, M. Giroud, A. Beley, C. Marie, J. Neurochem. 77 (2001) 408.
[32] J.A. Contreras, M. Karlsson, T. Østerlund, H. Laurell, A. Svensson, C. Holm, J. Biol. Chem. 271 (1996) 31426.
[33] N. Okada, Y. Tsukada, S. Nakagawa, H. Mizuguchi, K. Mori, T. Saito, T. Fujita, A. Yamamoto, T. Hayakawa, T. Mayumi, Biochem. Biophys. Res. Commun. 282 (2001) 173.
[34] C. Hay, H. De Leon, J.D. Jafari, J.L. Jakubczak, C.A. Mech, P.L. Hallenbeck, S.K. Powell, G. Liau, S.C. Stevenson, J. Vasc. Res. 38 (2001) 315.
[35] M.K. Magnusson, S.S. Hong, P. Boulanger, L. Lindholm, J. Virol. 75 (2001) 7280.
[36] H. Ghandehari, R. Sharan, W. Rubas, W.M. Killing, J. Pharm. Pharm. Sci. 4 (2001) 32.
[37] M.L. Lopez-Rodriguez, B. Vicente, X. Deupi, S. Barrondo, M. Olivella, M.J. Morcillo, B. Behamu, J.A. Ballesteros, J. Salles, L. Pardo, Mol. Pharmacol. 62 (2002) 15.
[38] M.T. Makhija, V.M. Kulkarni, J. Comput. Aided Mol. Des. 15 (2001) 961.
[39] I. Halperin, B. Ma, H. Wolfson, R. Nussinov, Proteins 47 (2002) 409.
[40] M. Glick, D.D. Robinson, G.H. Grant, W.G. Richards, J. Am. Chem. Soc. 124 (2002) 2337.
[41] J. Zhu, H. Fan, H. Liu, Y. Shi, J. Comput. Aided Mol. Des. 15 (2001) 979.
[42] R. Bitetti-Putzer, D. Joseph-McCarthy, J.M. Hogle, M. Karplus, J. Comput. Aided Mol. Des. 15 (2001) 935.
[43] A.W. Ravna, O. Edvardsen, J. Mol. Graph. Model. 20 (2001) 133.
[44] O.A. Santos-Filho, R.K. Mishra, A.J. Hopfinger, J. Comput. Aided Mol. Des. 15 (2001) 787.
[45] M.J. Frisch, G.W. Trucks, H.B. Schlegel, P.M. W. Gill, B.G. Johnson, M.A. Robb, J.R. Cheeseman, T. Keith, G.A. Petersson, J.A. Montgomery, K. Raghavachari, M.A. Al-Laham, V.G. Zakrzewski, J.V. Ortiz, J.B. Foresman, J. Cioslowski, B.B. Stefanov, A. Nanayakkara, M. Challacombe, C.Y. Peng, P.Y. Ayala, W. Chen, M.W. Wong, J.L. Andres, E.S. Replogle, R. Gomperts, R.L. Martin, D.J. Fox, J.S. Binkley, D.J. Defrees, J. Baker, J.P. Stewart, M. Head-Gordon, C. Gonzalez, J.A. Pople, GAUSSIAN 94, Revision D.2, Gaussian Inc., Pittsburgh PA, 1995.
[46] M.J. Frisch, G.W. Trucks, H.B. Schlegel, G.E. Scuseria, M.A. Robb, J.R. Cheeseman, V.G. Zakrzewski, J.A. Montgomery, Jr., R.E. Stratmann, J.C. Burant, S. Dapprich, J.M. Millam, A.D. Daniels, K.N. Kudin, M.C. Strain, O. Farkas, J. Tomasi, V. Barone, M. Cossi, R. Cammi, B. Mennucci, C. Pomelli, C. Adamo, S. Clifford, J. Ochterski, G.A. Petersson, P.Y. Ayala, Q. Cui, K. Morokuma, D.K. Malick, A.D. Rabuck, K. Raghavachari, J.B. Foresman, J. Cioslowski, J.V. Ortiz, A.G. Baboul, B.B. Stefanov, G. Liu, A. Liashenko, P. Piskorz, I. Komaromi, R. Gomperts, R.L. Martin, D.J. Fox, T. Keith, M.A. Al-Laham, C.Y. Peng, A. Nanayakkara, C. Gonzalez, M. Challacombe, P.M.W. Gill, B.G. Johnson, W. Chen, M.W. Wong, J.L. Andres, M. Head-Gordon, E.S. Replogle, J.A. Pople, GAUSSIAN 98, Revision A.x, Gaussian Inc., Pittsburgh, PA, 1998.
[47] M. Tarditi, M.W. Klipfel, A.M. Rodriguez, F.D. Suvire, G.A. Chasse, Ö. Farkas, A. Perczel, R.D. Enriz, J. Mol. Struct. (Theochem) 545 (2001) 29.
[48] M.F. Masman, M.G. Amaya, A.M. Rodriguez, F.D. Suvire, G.A. Chasse, Ö. Farkas, A. Perczel, R.D. Enriz, J. Mol. Struct. (Theochem) 543 (2001) 203.
[49] M.N. Barroso, E.S. Cerutti, A.M. Rodriguez, E.A. Jauregui, Ö. Farkas, A. Perczel, R.D. Enriz, J. Mol. Struct. (Theochem) 548 (2001) 21.
[50] C.M. Deane, F.H. Allen, R. Taylor, T.L. Blundell, Protein Engng 12 (1999) 1025.